A Three-Dimensional Mechanistic Model of *Prorocentrum minimum* Blooms in Eutrophic Chesapeake Bays

Fan Zhang, Ming Li*, Patricia M. Glibert and So Hyun (Sophia) Ahn

University of Maryland Center for Environmental Science, Horn Point Laboratory, PO Box 775, Cambridge, Maryland 21613, U.S.A.

Submitted to *Science of the Total Environment*

*Correspondence to: Ming Li, Horn Point Lab, University of Maryland Center for Environmental Science, Cambridge, Maryland 21613, U.S.A. Email: mingli@umces.edu.

Abstract

Planktonic *Prorocentrum,* a common harmful dinoflagellate, are increasing in frequency, duration, and magnitude globally, as exemplified by the number of blooms of *P. minimum* in Chesapeake Bay that have nearly doubled over the past 3 decades. Although the dynamics of transport and seasonal occurrence of this species have been previously described, it has been challenging to predict the timing and location of *P. minimum* blooms in Chesapeake Bay. We developed a new three-dimensional mechanistic model of this species that integrates physics, nutrient cycling and plankton physiology and embedded it within a coupled hydrodynamic-biogeochemical model originally developed for simulating water quality in eutrophic estuarine and coastal waters. Hindcast simulations reproduced the observed time series and spatial distribution of cell density, in particular capturing well its peak in May in the mid-to-upper part of the estuary. Timing and duration of the blooms were mostly determined by the temperature-dependent growth function, while mortality due to grazing and respiration played a minor role. The model also reproduced the pattern of overwintering populations, which are located in bottom waters of the lower Bay, and are transported upstream in spring by estuarine flow. Blooms develop in the mid-upper parts of the estuary when these transported cells encounter high nutrient concentrations from the Susquehanna River and favorable light conditions. Diagnostic analysis and model-sensitivity experiments of nutrient conditions showed that high nitrogen:phosphorus conditions favor bloom development. The model also captured the observed interannual variations in the magnitude and spatial distribution of *P. minimum* blooms.

Keywords: harmful algal blooms; *Prorocentrum minimum*; eutrophication; estuary; mechanistic model;

1. Introduction

The over-enrichment of Chesapeake Bay by nutrients has been well recognized and documented (e.g., Fisher et al., 1992, 2006; Boesch et al., 2001; Hagy et al., 2004; Kemp et al., 2005; Brush, 2009). Between the 1950s and 1980s there was an increase in chlorophyll *a* (Chl *a*), corresponding to trends in nitrogen (N) loading to the Bay during this period (Kemp et al., 2005), but since the 1990s, these increases have slowed (Harding et al., 2016). Although most of the Chl *a* is dominated by diatoms, especially in spring, analysis of sediment cores has indicated that relative abundances of dinoflagellates, cyanobacteria, and small flagellates have increased significantly during the last half of the 20th century (e.g., Zimmerman and Canuel, 2002). Among the dinoflagellates that have increased in recent years are several harmful algal bloom (HAB) taxa, which are now more frequent, and of significantly higher densities, than several decades ago (Glibert et al., 2001; Kemp et al., 2005; Anderson et al., 2008; J. Li et al., 2015). For example, the dinoflagellate *Prorocentrum minimum* is now observed in blooms at densities 3-fold higher than were noted in the 1970's, reaching 10^8 cells L^{-1} (Tyler and Seliger, 1978; Tango et al., 2005; J. Li et al., 2015).

Earlier estuary-wide field surveys suggested that *P. minimum* originates from the lower Chesapeake Bay in winter (no known cysts in sediments), moves upstream and develops into a bloom in the mesohaline region in late spring (Tyler and Seliger 1978, 1981). Observations of *P. minimum* since 1985 have been mostly based on biweekly or monthly measurements at a limited number of water quality monitoring stations (Tango et al. 2005; J. Li et al., 2015) and do not provide as complete a picture of the bloom distribution over the entire estuary as did the earlier studies. Although the 3-fold increases in the cell density over the past few decades have been shown to be correlated with the increases in nutrient loading (Tango et al., 2005; J. Li et al.,

2015), a recent analysis of the monitoring data found that the peak bloom location shifts upstream or downstream in response to internannual variations in river flows, pointing to the possible effect of climate variability (M. Li et al., 2020). Understanding the mechanisms driving the long-term trend and interannual fluctuations of *P. minimum* biomass requires the development of a mechanistic model to complement the retrospective data analysis.

Planktonic *Prorocentrum* species are among the most commonly recognized harmful algae that are increasing in frequency, duration, and magnitude globally (Heil et al., 2005; Glibert et al., 2008; 2012); as of 2003, at least 56 species within the genus *Prorocentrum* were known to populate estuarine and marine waters (Gómez, 2005) and of these, at least six species have been shown to form high biomass blooms (Glibert et al., 2012 and references therein). Blooms of *P. minimum* have been associated with anoxic/hypoxic events, finfish kills, aquaculture shellfish kills and submerged aquatic vegetation losses (Heil et al., 2005). *Prorocentrum* sp. has flourished in the estuaries of the U.S. East Coast as these systems have become increasingly eutrophic (Glibert et al., 2012 and references therein).

Despite the increasing prevalence of *Prorocentrum* blooms in Chesapeake Bay and elsewhere, only a handful of modeling efforts have been reported for this HAB taxon. Most of these efforts have been based on statistical or empirical models constructed from observational data (e.g., Pertola et al., 2005; Xu et al., 2010; Brown et al., 2013; M. Li et al., 2020). Empirical-statistical models have been used for studying various HAB species, including toxic *Pseudo-nitzschia* blooms in Santa Barbara Channel (Anderson et al., 2009) and in Chesapeake Bay (Anderson et al., 2010), *Karenia brevis* blooms in the Gulf of Mexico (Stumpf et al., 2009), cyanobacterial blooms in Lake Erie (Obenour et al., 2014), *Phaeocystis globosa* blooms in Dutch coastal waters (Blauw et al., 2010), and *Dinophysis acuminata* blooms in a coastal embayment in

Ireland (Raine et al., 2010). These models are only interpretable within the limits of the observational data used to generate them (Franks, 2018), making them less reliable for predicting HABs under a different set of forcing conditions such as a changing climate (Ralston and Moore, 2020; Glibert et al., 2020).

Coupling HAB models to three-dimensional circulation models is still a relatively nascent field (Franks, 2018). For HABs where physical transport provides the dominant control on bloom distribution, a Lagrangian approach, tracking passive particles or individuals with behavior, has proven to be effective (McGillicuddy, 2010). Giddings et al. (2014) used particle tracking models to investigate two transport pathways to the HAB hotspots on the U.S. Pacific Northwest. Y. Li et al. (2014) released particles nearly continuously at 7 sites previously suspected to be potential source regions of *Alexandrium fundyense* and tracked them as they were moved in the Gulf of Maine. Pinto et al. (2016) tracked passive particles in a 3D circulation model of the Iberian coast and showed the possibility of local HAB presence based on transport of toxic cells from distant point sources.

Another modeling approach applied to many HABs is process or mechanistic models that are based on mathematical equations that describe HAB growth in terms of mathematical formulation of biogeochemical and physiological processes such as nutrient uptake, photosynthesis and grazing (Franks, 2018; Flynn and McGillicuddy, 2018). For example, Gillibrand et al. (2016) coupled a 3D circulation model of Northwest European continental shelf to an individual-based model of *Karenia mikimotoi* that simulates temperature-dependent growth, mortality and photoaxis. In addition to the Lagrangian approach, an Eulerian approach was developed to model the germination and growth rates of *Alexandrium fundyense* in the Gulf of Maine (Stock et al., 2005; He et al., 2008; McGillicuddy et al., 2011).

For HABs in which eutrophication is a major driver for their proliferation (Glibert et al., 2005), a mechanistic model needs to explicitly consider nutrient input, nutrient kinetics and plankton physiology (Glibert et al., 2010, 2020; Flynn and McGillicuddy, 2018). Allen et al. (2001) coupled a 3D circulation model to an ecosystem model (the European Regional Seas Ecosystem Model or ERSEM), and used this coupled model to predict high biomass algal bloom events on the Northwest European shelf. Although the model did not resolve specific algal species, it was able to predict blooms captured in satellite remote sensing of Chl *a* since the harmful algal species dominated the total phytoplankton biomass during the bloom periods. Vanhoutte-Brunier et al. (2008) added a specific module for toxic *Karenia mikimotoi* to ERSEM and simulated the *K. mikimotoi* blooms in English Channel. A similar approach was used here to develop a mechanistic model for *P. minimum*. That is, a rhomboid strategy was used, characterizing the individual HAB taxa against a background of other functional groups. This is necessary because although eutrophication drives *P. minimum* blooms in Chesapeake Bay (J. Li et al., 2015), dinoflagellates like *P. minimum* typically only constitute 20-30% of the total phytoplankton biomass, as diatoms dominate biomass much of the year (Harding et al., 2015). Therefore, a 3D coupled biophysical model that not only simulates nutrient dynamics and total phytoplankton biomass but also treats specific HAB specie as a separate state variable is needed.

Many questions regarding *P. minimum* bloom dynamics remain unanswered. Is the timing of the *P. minimum* bloom regulated by temperature-dependent growth rate, light availability, nutrient availability and/or grazing? Why does the bloom occur most frequently in the upper and mid Bay region even though *P. minimum* originates from the lower Bay? Is *P. minimum* growth limited by nitrogen or phosphorous or both? The 3D mechanistic model of *P. minimum* applied here integrates physics, nutrient cycling, physical factors and nutrient

physiology, and is used to address the above questions. This model was coupled to an existing hydrodynamic-biogeochemical model that simulates the hydrodynamics and the general nutrient dynamics of Chesapeake Bay. It allowed us to consider multiple nutrients and seasonal dynamics. The overall goal of this modeling study is to gain a better understanding of physical and biogeochemical processes that regulate the seasonal dynamics of *P. minimum* blooms and their geographic distributions in the estuary.

2. Methods

The mechanistic model for *P. minimum* was built upon a 3D coupled hydrodynamic-biogeochemical modeling framework that was previously developed for investigating nutrient cycling and water quality in shallow water shelf and estuaries like Chesapeake Bay (Testa et al., 2014; M. Li et al., 2016). The hydrodynamic model is based on the Regional Ocean Modeling System (ROMS) (Shchepetkin and McWilliams, 2005, 2009a, 2009b; Haidvogel et al., 2008), and the biogeochemical model is based on the Row Column Aesop (RCA) structure (Isleib et al., 2007; DiToro, 2001). In this study we developed a new model for *P. minimum* and incorporated it into ROMS-RCA, and have termed this new integrated model ROMS-RCA-*Prorocentrum*.

2.1 ROMS configuration

The ROMS hydrodynamic model was configured to cover the Chesapeake Bay and its adjacent shelf (M. Li et al., 2005). In the horizontal direction, the curvilinear coordinate system has 80 x 120 grid points, with a grid resolution of 590-1000 m (Fig. 1a). In the vertical direction, the sigma coordinate system has 20 evenly distributed vertical levels. ROMS is forced by freshwater discharge at river heads, water levels at the open boundary, and heat and momentum

flux across the sea surface. The freshwater input was prescribed for the 8 major tributaries of Chesapeake Bay, based on measurements at US Geological Survey gaging stations. The offshore boundary water level consists of tidal and non-tidal components. The tidal component was provided by TPXO7 (Egbert and Erofeeva, 2002), and non-tidal component was extracted from daily sea level measured at Duck, North Carolina, by National Oceanic and Atmospheric Administration (NOAA). The air-sea heat flux and momentum flux were calculated using the North America Regional Reanalysis (NARR) data. The vertical eddy viscosity and diffusivity were parameterized using the k-kl turbulence closure scheme with the background value set at 1 x 10^{-6} $m^2 s^{-1}$, and the horizontal eddy viscosity and diffusivity were set to be constant (1 $m^2 s^{-1}$). The ROMS model was initialized using climatological temperature and salinity conditions and run for a spin-up period of 3 years. This hydrodynamic model was previously validated against the observational data (e.g., M. Li et al., 2005; Zhong and Li, 2006; M. Li et al., 2006; Xie and Li, 2018; Xie et al., 2018).

2.2 RCA Configuration

The RCA biogeochemical model is coupled to the ROMS hydrodynamic model in an offline mode, and uses hourly averages of temperature, salinity, and transport terms from ROMS to drive the biogeochemical variables (Testa et al., 2014). The RCA has a water-column component (Isleib et al., 2007; Zhang and Li, 2010) and a two-layer sediment diagenesis model (DiToro, 2001; Brady et al., 2013). The water-column model includes state variables representing dissolved inorganic N, P, and Si, particulate and dissolved organic N and P, and dissolved O_2. In its typical configuration, RCA simulates two generic phytoplankton groups with different kinetics: one representing a winter-spring “diatom” group and one representing a

summer "dinoflagellates" group. RCA is driven by loads of dissolved and particulate nutrients from river flows. In-river nutrient concentrations were obtained from monitoring stations within the 8 major tributaries entering the ROMS-RCA domain (https://www.chesapeakebay.net/what/data). Nutrient concentrations at the offshore boundary on the shelf were acquired from the World Ocean Atlas (Garcia et al., 2013) and Filippino et al. (2011). The ROMS-RCA model has been previously validated and used in several modeling studies (Testa et al., 2014; Li et al., 2016; Testa et al., 2017; Ni et al., 2020).

2.3 Prorocentrum minimum parameterization

To embed *P. minimum* within RCA, a rhomboid strategy was used (DeYoung et al., 2004; Mitra and Davis, 2010): that is, *P. minimum* are modeled individually while the other plankton assemblages are represented by the aggregate functional classes, namely the winter-spring diatom group and summer dinoflagellates group. The rate of growth of *P. minimum* is simulated by solving the following equation:

$$\frac{d(proro)}{dt} = G * proro - R_{res} * proro - R_{gz} * proro^2 \quad (1)$$

where *proro* is the biomass of *P. minimum* measured by carbon (C, unit: mgC L^{-1}). The growth rate (G) of *P. minimum* depends on temperature (T), light, and nutrient concentrations in the water, such that:

$$G = G_T * G_{par} * G_N \quad (2)$$

where the specific growth rate

$$G_T = \begin{cases} G_p e^{-\beta_1 (T - T_{opt})^2} & (T \le T_{opt}) \\ G_p e^{-\beta_2 (T - T_{opt})^2} & (T \ge T_{opt}) \end{cases} \quad (3)$$

is related to the maximum growth rate G_p (unit of d^{-1}) through the temperature-dependent functions shown above. T_{opt} is the optimal temperature for the maximum growth; and β_1 and β_2 are shape factors characterizing the window of optimal growth.

The effect of light availability on *P. minimum* growth (G_{par}) is parameterized using the hyperbolic function given by:

$$G_{par} = \frac{\alpha * PAR}{\sqrt{G_T{}^2 + (\alpha * PAR)^2}} \quad (4)$$

in which α is the slope of the P-I curve (in unit of ly^{-1}); PAR is photosynthetically active radiation (in unit of ly d^{-1}) and attenuates with depth (H) exponentially:

$$PAR = PAR_{surf} e^{-k_d H} \quad (5)$$

where PAR_{surf} is the surface light intensity and k_d is the light extinction coefficient.

The effects of nutrient limitation on *P. minimum* growth are parameterized by:

$$G_N = min(G_{DIN},\ G_{DIP}) = min(\frac{DIN}{DIN+K_{mn}}, \frac{DIP}{DIP+K_{mp}}) \quad (6)$$

where DIN is dissolved inorganic N including NO_3^-+NO_2^- (hereafter NO_3^-) and NH_4^+; DIP is dissolved inorganic phosphorous (hereafter PO_4^{3-}); K_{mn} and K_{mp} are the half saturation constants corresponding to DIN and DIP, respectively; and $G_{DIN} = \frac{DIN}{DIN+K_{mn}}$ and $G_{DIP} = \frac{DIP}{DIP+K_{mp}}$.

The mortality rate of *P. minimum* consists of 2 parts: grazing ($R_{gz} * proro^2$) and respiration ($R_{res} * proro$). Since zooplankton are not explicitly modeled in RCA, R_{gz} is parameterized as a temperature dependent function:

$$R_{gz} = k_{gz} * \theta_{gz}{}^{(T-20)} \quad (7)$$

where k_{gz} is the grazing rate at 20°C and θ_{gz} is the temperature coefficient. R_{res} is parameterized by:

$$R_{res} = k_{rb} * \theta_{rb}{}^{(T-20)} \quad (8)$$

where k_{rb} is the respiration rate at 20°C, and θ_{rb} is the temperature coefficient.

Values of the parameters in Equations (1)-(8) are determined according to published physiological experiments on *P. minimum* (Table 1) and numerical sensitivity-analysis experiments. For example, the maximum growth rate G_p reported in the literature ranges from 0.12 to 2.84 d^{-1} (Heil et al., 2005), and our numerical sensitivity analysis showed that $G_p = 2.5$ d^{-1} (Smayda, 1996) provided the best estimate for the bloom size of *P. minimum* in Chesapeake Bay. Earlier studies of *P. minimum* in Chesapeake Bay (Tyler and Seliger, 1981) and in the Mediterranean Sea (Grzebyk and Berland, 1996) suggested an optimal temperature growth around ~25 °C (Fig. 2a). However, recent field observations of *P. minimum* in Chesapeake Bay clearly showed highest bloom density at a temperature range between 13 and 25 °C (Tango et al., 2005; Fig. 2b). Herein $T_{opt} = 20$ °C provided a good overall fit to all four data sets available, including those reported in Lomas and Glibert (1999). For α, the value obtained from the spatially- and annually-averaged P-I curve slope for phytoplankton in Chesapeake Bay was used (Harding et al., 2002; M. Li et al., 2009). The reported half saturation coefficient K_{mp} for DIP varied over a wide range, suggesting the presence of both low-and high-affinity transporters depending on nutrient conditions. In an earlier study, Cembella et al. (1984) reported $K_{mp} = 1.96$ μM for *P. minimum*. However, the batch culture experiments by Ou et al. (2008) estimated $K_{mp} =$ 0.25 μM for a similar species, *P. donghaiense*. Jiang et al. (2019) fitted a nutrient kinetic model to culture growth data on *P. donghaiense* and found low K_{mp} values. It appears that *P. minimum* in Chesapeake Bay has high-affinity transporters and thus a value of $K_{mp} = 0.03$ μM was selected in the control model run, but additional model runs with other values of K_{mp} were conducted. Since the swimming speed of *P. minimum* has a mean speed of 51.3 ± 27.9 μm/s (Sohn et al., 2013), it was not considered in the model.

251

252 *2.4 Hindcast simulations*

253 Herein, ROMS-RCA-*Prorocentrum* model was first used to conduct a hindcast
254 simulation for a 10-year period between 2002 and 2011. The hydrodynamic modeling
255 component was initialized from a spin-up run over 2000-2001, and the biogeochemical modeling
256 component was initialized on January 1 every year, as done in Testa et al. (2014), M. Li et al.
257 (2016) and Ni et al. (2020). Observations of *P. minimum* were limited during winter; with only
258 three monitoring sites recording cell density in the main stem of the Bay. To construct the initial
259 condition of *P. minimum* for the entire estuary, the limited winter data were interpolated using
260 the distribution reported in the estuary-wide surveys reported in Tyler and Seliger (1978). Model
261 sensitivity-analysis experiments showed that the prediction of *P. minimum* blooms is insensitive
262 to the initial condition as long as a small seed population exists at the beginning of the year (see
263 Section 3.4 below). Finally, the boundary conditions for *P. minimum* at the river heads and
264 continental shelf were set to 0 as there are no (or very limited data) observational evidence
265 suggesting that these are significant sources of *P. minimum* into the estuary.

266

267 *2.5 Model skill assessment*

268 Taylor (Taylor, 2001) and Target (Jolliff et al., 2009) diagrams were constructed to
269 quantify the model's skill in predicting the time series of NO_3^- and PO_4^{3-} at a number of
270 monitoring stations in the estuary. In the Taylor diagram, the correlation coefficient r, the
271 centered root-mean-square error E, and the ratio σ_n of the standard deviations of the model-
272 predicted field and the observed field are displayed by the location of one point (representing the
273 model field) in relation to the reference point (representing the observed field). The Target

diagram provides summary information about the pattern statistics as well as the bias, thus allowing for an assessment of their respective contributions to the total rms. The normalized bias is defined as the ratio of the bias to the observed standard deviations.

3. Results

The ROMS-RCA-*Prorocentrum* was examined in 5 ways: 1) comparison of predicted nutrient concentration, Chl *a* and *P. minimum* abundances with observations; 2) seasonal dynamics of *P. minimum*; 3) environmental factors impacting blooms; 4) model sensitivity, and 5) model performance over multiple years.

3.1 Comparison with observations

To illustrate the model comparisons with Chesapeake Bay Program (CBP) monitoring program data, the year 2006 is first used, given the density of available data for this year and the observed bloom (Fig. 3a). Nutrient concentrations and Chl *a* were averaged over 3-month periods to produce seasonal means for both surface and bottom waters. The distributions of NO_3^-, NH_4^+, PO_4^{3-} and Chl *a* in the estuary were captured well by ROMS-RCA-*Prorocentrum* (Fig. 3).

The model-predicted NO_3^- follows the observed pattern well (Figs. 3b1-3b4 and 3f1-3f4). Concentrations of NO_3^- displayed a strong longitudinal gradient, decreasing from a maximum at the head of the estuary to near zero concentration in the lower Bay, as the Susquehanna River in the northernmost of the estuary delivers most of this external inorganic dissolved nitrogen. The maximum NO_3^- in the surface water was about 30 μM during the low-flow summer season but averaged around 60 μM during the other three seasons. The bottom water NO_3^- followed a similar longitudinal trend but at lower concentration. Concentrations of NH_4^+ were generally

297 higher in the bottom water than in the surface water and showed weaker longitudinal variations
298 than NO_3^- (Figs. 3c1-3c4 and 3g1-3g4). Since NH_4^+ was mostly generated from remineralization
299 of organic materials in the water column or from the efflux from the sediment (Testa et al., 2014),
300 NH_4^+ was higher during summer, reaching a maximum of ~15 μM in the bottom water and ~5
301 μM in the surface water.

302 Concentrations of PO_4^{3-} also decreased from the head to the mouth of estuary (Figs. 3d1-
303 3d4 and 3h1-3h4). During spring and winter, most of PO_4^{3-} came from the rivers and had
304 concentrations less than ~0.5 μM, with small differences between the surface and bottom waters.
305 During summer and fall, most of the PO_4^{3-} was produced through internal biogeochemical
306 cycling, with the bottom water PO_4^{3-} concentrations reaching 2 μM and the surface water PO_4^{3-}
307 reaching 1 μM. During the summer, PO_4^{3-} in the bottom water was highest in the middle bay, as
308 PO_4^{3-} efflux from the sediment accelerated under the hypoxic condition (e.g., Hagy et al., 2004;
309 Kemp et al., 2005, 2009; Testa et al., 2014; M. Li et al., 2016; Ni et al., 2020).

310 The coupled model also captured the seasonal dynamics and longitudinal distribution of
311 the total phytoplankton biomass (as measured by Chl *a*) (Figs. 3e1-3e4 and 3i1-3i4). Chl *a* was
312 highest during spring and decreased along the center axis from the upper to lower Bay. Bottom
313 water Chl *a* was also high due to the sinking of spring diatoms. Surface Chl *a* was nearly as large
314 during summer and reached a maximum in the mid-Bay, but the bottom Chl *a* was much lower
315 as the summer assemblage was less likely to sink. Chl *a* in fall and winter were lower. The model
316 did a reasonable job capturing the temporal and spatial variations of Chl *a* in Chesapeake Bay.

317 The Taylor and Target diagrams (Fig. 4) quantify the model's skill in predicting the time
318 series of NO_3^- and PO_4^{3-} at a number of monitoring stations in the estuary. In the Taylor diagram,
319 the correlation coefficient r ranges from 0.7 to 0.9 for NO_3^- and ranges from 0.5 to 0.8 for PO_4^{3-},

indicating that the model captured the phase of nutrient seasonal variation well (Figs. 4a and 4c). The normalized standard deviation σ_n for NO_3^- is about 1 at stations CB4.1C, CB4.2C, CB4.3C and CB5.2, but is about 0.7-0.8 at CB3.1 and CB3.3C, indicating that the model under-predicts the observed seasonal variations in NO_3^- there (Fig. 4a). Values of σ_n for PO_4^{3-} straddle 1 at CB4.1C, CB4.2C, CB4.3C and CB5.2, but are lower than 1 (0.55-0.7) at CB3.1 and CB3.3C (Fig. 4c). In the Target diagram, the normalized bias was mostly positive (0 - 0.5) for NO_3^- and negative (-0.5 - 0) for PO_4^{3-}, suggesting that NO_3^- was slightly overpredicted and PO_4^{3-} was slightly under-predicted. The normalized root-mean-squared error fell with the range of 0.5 - 1, corroborating the robust predictive skill of the model.

The model unit for *P. minimum* is carbon, mg C L^{-1}, although the observations are reported as cell numbers. To compare the model data with the cell density in the monitoring data, a cell C content of 293 pg C $cell^{-1}$ (based on Dam and Colin, 2005), was used to convert the predicted C concentrations to cell numbers. When doing so, the predicted time series of *P. minimum* cell abundances were in agreement with the observed cell density at the monitoring stations (Fig. 5), including the three stations in the main stem of the Bay (CB3.3C, CB4.3C, CB5.2), one station in the Potomac River (largest tributary in the western shore, LE2.2), and one station in the Choptank River (largest tributary in the eastern shore, ET5.2; Fig. 1b).

The ROMS-RCA-*Prorocentrum* model captured most of the seasonal variation of the observed *P. minimum* concentrations, including the often-observed peak bloom in May and the relative low concentration during summer. In the mainstem of the Bay, the two stations in the upper and middle parts of the Bay (CB3.3C and CB4.3C) recorded blooms during the month of May, with maximum cell densities reaching or exceeding 10^6 cells L^{-1}. The cell density at CB5.2 in the lower part of the Bay was much lower. In contrast, *P. minimum* concentration at the two

343 tributary stations in the mid-Bay was much higher, with the cell density reaching (2-3) × 10^6
344 cells L^{-1} (Figs. 5d and 5e). At CB4.3C, LE2.2 and ET5.2, a second bloom appeared in late fall.

345 Bloom size was also well simulated at the two upper Bay stations, but was overestimated
346 at the downstream station. The model underestimated the bloom size at the tributaries, especially
347 at ET5.2, likely due to coarse model resolution in the Choptank River. Overall, ROMS-RCA-
348 *Prorocentrum* captured the seasonal variation and bloom size of *P. minimum* in most parts of the
349 Bay. In terms of predictive skill, the r value was between 0.64 and 0.86 and the overall skill
350 score (Warner et al., 2005) was between 0.57 and 0.92 in the middle and upper parts of the Bay
351 where significant blooms was observed (Table 2). The model had a lower score of 0.23 at the
352 lower Bay station CB 5.2.

353

354 *3.2 Seasonal dynamics of* P. minimum

355 The model herein reproduces well the conceptual notion that there are over-wintering
356 populations of *P. minimum* in the lower Bay, and that a bloom develops in the upper and middle
357 parts of Chesapeake Bay as spring progresses and as these cells are transported upstream. The
358 3D seasonal dynamics of *P. minimum* in Chesapeake Bay were simulated by ROMS-RCA-
359 *Prorocentrum,* using 2006 again as the example.

360 During January and February, *P. minimum* concentrations were low throughout the Bay,
361 but a small population was found in the lower Bay, particularly along the western tributaries –
362 the James and York Rivers (Figs. 6a-6b). In March and April, *P. minimum* started to form in the
363 middle parts of the Bay and in the neighboring tributaries (Figs. 6c-6d). During May, a *P.*
364 *minimum* bloom developed in the middle and upper parts of the estuary, covering the mainstem
365 between 38 and 39.2 ^{o}N, as well as the Potomac River (Fig. 6e). At this time, the cell density

366 reached over 10^6 cells L^{-1} in the mid- to upper Bay, while in the lower Bay much lower cell
367 concentrations, < 0.3×10^6 cells L^{-1}, were observed. After peaking in May, the concentration of
368 *P. minimum* dropped quickly and remained at low levels (~1×10^3 to 1×10^4 cells L^{-1}) until
369 October (Figs. 6f-6j). Then, in November a second bloom started to form in the northern part of
370 the Bay between 38 and 39.2°N, but the cell density was lower than in May (5×10^5 to 10^6 cells
371 L^{-1}). These predicted *P. minimum* distributions are in agreement with the observations at the
372 monitoring stations (Fig. 5); specifically during May, when stations north of CB 4.3C
373 experienced blooms of ~1×10^6 cells L^{-1}, while stations downstream had much lower
374 concentrations (< 1×10^5 cells L^{-1}). The two tributaries also had larger blooms than stations in
375 the southern part of the main channel.

376 Examination of *P. minimum* distribution in the along-channel section, together with the
377 estuarine circulation field, provides further insights into the seasonal dynamics and spatial
378 distribution of this HAB species (Fig. 7). During the beginning of 2006, a small population of *P.*
379 *minimum* cells were located in the shallow lower Bay and mostly in the bottom water (Figs. 7a-
380 7b). Starting in March, this bottom population was advected upstream by the landward flow in
381 the bottom layer (Fig. 7c). By April, significant population extended over the lower and mid-Bay
382 regions (Fig. 7d). During March and April, the highest *P. minimum* concentration remained in
383 the bottom waters, but vertical mixing began to inject *P. minimum* cells upward into sun-lit
384 surface water. These cells then grew rapidly, as they had adequate light and nutrients. A large *P.*
385 *minimum* then bloom developed in May, with the highest concentration of 1.7×10^6 cells L^{-1} at
386 ~180-230 km from the mouth of the estuary (Fig. 7e). The bloom occupied a depth range down
387 to 10-15 m. The bloom almost completely disappeared in June, with small residual populations
388 remaining in the upper Bay. After the peak bloom, *P. minimum* was quickly removed from the

389 water column throughout the bay and was hardly detected during summer and early fall (Figs. 7f-
390 7j). In November, *P. minimum* cells appeared again in the middle-upper part of the Bay with a
391 maximum concentration of ~0.4 × 10^6 cells L^{-1} in the surface water (Fig. 7k). The seaward flow
392 in the surface layer transported these cells downstream, and a second bloom with a maximum
393 concentration of ~0.9 × 10^6 cells L^{-1} can be found in the mid-Bay (Fig. 7l).

394 The model allows a more detailed look into the rapid development of the *P. minimum*
395 bloom in spring (Fig. 8). On April 10, highest cell densities were found in the lower-Bay but a
396 plume of *P. minimum* cells was beginning to be advected upstream by the estuarine return flow
397 in the bottom layer (Fig. 8a). Within 10 days, some of these cells were mixed upwards into the
398 sun-lit surface layer (Fig. 8b). A bloom started to develop on April 30 (Fig. 8c) and peaked
399 around May 5 (Fig. 8d). The bloom area shrank in size by May 10 (Fig. 8e) and even more by
400 May 30 (Fig. 8f).

401

402 *3.3.* In silico *tests on the timing, duration and spatial distribution of* P. minimum *blooms*

403 To understand why the bloom appeared in the particular regions of the mid- to upper Bay,
404 the along-channel distributions of NO_3^- and PO_4^{3-} during spring were compared against the *P.*
405 *minimum* distribution (Fig. 9). As the Susquehanna River flow increased during the spring, it
406 delivered NO_3^- and PO_4^{3-}, resulting in strong longitudinal gradients. At the head of the estuary,
407 NO_3^- concentrations were 50-100 μM, and decreased to 10-30 μM in the mid-Bay, and 5 μM in
408 the lower Bay and also decreased from April to May due to phytoplankton uptake. PO_4^{3-}
409 concentrations were ~0.5 μM in the upper Bay, decreased to ~0.2 μM in the mid-Bay and 0.05
410 μM in the lower Bay. Overlaying NO_3^- and PO_4^{3-} distributions with those of *P. minimum*
411 suggests that the *P. minimum* bloom developed in the upper-middle parts of the estuary due to

412 high nutrient availability. However, this does not explain why blooms did not occur in the
413 uppermost part of the estuary (250-300 km from the mouth of the Bay).

414 To further resolve the spatial distribution of *P. minimum*, we used the model outputs to
415 conduct a diagnostic analysis of various terms regulating the growth of *P. minimum*, as shown in
416 Eq. (1). Given the consistently high concentrations, N was not limiting over most of the upper
417 and mid-Bay, with G_{DIN} in the range of 0.9-1 (Fig. 10a). On the other hand, concentrations of P
418 were more variable, and G_{DIP} was considerably smaller than G_{DIN} except in the shallow upper
419 Bay (Fig. 10b). In particular, G_{DIP} in the surface layer (down to ~10 m depth) dropped to ~0.3
420 towards the south. A comparison between G_{DIN} and G_{DIP} suggests that P was the more likely
421 limiting nutrient for *P. minimum* growth. The specific growth rate G_T [Eq. (3)] is a temperature-
422 dependent function and was higher in the surface water than in the bottom water (Fig. 10c). The
423 longitudinal difference was relatively weak except in a region of strong vertical mixing (in the
424 upper Bay) which resulted in lower temperature in surface waters. The light limitation function
425 G_{par} [Eq. (4)] showed strong depth dependence (Fig. 10d). It dictated no or very weak *P.*
426 *minimum* growth below 10 m depth. Due to high suspended sediment concentration and low light
427 penetration, G_{par} dropped to low values in the shallow upper Bay. This explains why the *P.*
428 *minimum* bloom did not occur there. Growth rate of *P. minimum* was highest in the region
429 between 180 and 230 km from the estuary's mouth and in the surface layer (Fig. 10e), consistent
430 with the distribution of *P. minimum* population (Fig. 10f). No one-to-one correspondence was
431 expected, however, as the advection by the estuarine circulation and turbulent mixing
432 redistributed the biomass in the estuary.

433 Both the model results and the monitoring data at CBP stations showed that bloom only
434 lasted about one month. Such a short window for the bloom can be explained by comparing the

435 time series of the various terms in the growth function at a mid-Bay station CB4.1C (Fig. 11).
436 The surface temperature in Chesapeake Bay was 18-20^{o}C in May, close to the optimum
437 temperature for *P. minimum* growth (Fig. 11a). However, G_T decays exponentially away from the
438 optimal temperature [Eq. (3)] such that its peak value of (2.5 d^{-1}) in May was much higher than
439 its summer value of less than 0.5 d^{-1} (Fig. 11b). Together with the nutrient limitation (G_N) (Fig.
440 10c) and light limitation (G_{Par}) (Fig. 11d) at this mid-Bay location, the biomass growth rate
441 (defined as *G*proro*) of *P. minimum* displayed a sharp and narrow peak in May (0.75 mgC L^{-1}
442 day^{-1}) and dropped to near 0 during the summer months (Fig. 11e). This resulted in a bloom that
443 only lasted for a month (Fig. 8). The biomass growth reached a smaller second maximum in late
444 fall as the water temperature fell back into the optimal growth window again (Figs.11b and 11e),
445 leading to a fall bloom (Fig. 5).

446 The mortality rate of *P. minimum*, consisting of grazing rate and respiration rate, was
447 largely in sync with the time series of the growth rate but with a short phase lag of ~1 week (Figs.
448 11f-11g). In the model, loss of *P. minimum* due to grazing was made proportional to the
449 quadratic of *P. minimum* biomass in order to simulate the observed grazing rate on *P. minimum*
450 in Chesapeake Bay; while loss due to respiration is linearly proportional to biomass. As a result,
451 both the grazing and respiration rates were highly correlated to *P. minimum* cell concentration in
452 the time series. The mortality rate was much smaller than the growth rate. At the surface of CB
453 4.1C where *P. minimum* concentration was among the highest recorded, the biomass growth rate
454 was ~0.75 mg C day^{-1}, while mortality due to grazing (R_{gz}*$proro^2$) and respiration (R_{res}*$proro$)
455 were 0.06 mg C day^{-1} and 0.04 mg C day^{-1}, respectively (compare Figs. 11e-11g). This faster
456 biomass growth rate was essential to the formation of the *P. minimum* bloom. Furthermore, the
457 peak mortality lagged the peak biomass growth rate by about 1 week, suggesting that mortality

458 may have contributed to the decline of *P. minimum* bloom. Nevertheless, the duration of the
459 bloom was mostly determined by the temperature-dependent growth function and nutrient
460 limitation.

461 Two additional numerical experiments were conducted to explore nutrient limitation: one
462 removing DIN limitation [the first hyperbolic function in Eq. (6)]; one removing DIP limitation
463 [the second hyperbolic function in Eq. (6)]. The predicted *P. minimum* biomass from these two
464 model runs were compared with that obtained from the control model run that considered both
465 nutrients (Fig. 12). Compared to the control model run, the run without DIN limitation showed
466 similar annual maximum *P. minimum* concentrations in the northern part of the bay, but over-
467 predicted the concentration in the southern part of the bay (compare Figs. 12a and 12b). In the
468 monthly time series, both model runs predicted a peak bloom in May with similar maximum cell
469 concentrations (compare Figs. 12d and 12e). On the other hand, the experiment without DIP
470 limitation grossly over-predicted the maximum cell concentration by 2-5 fold (compare Figs. 12a
471 and 12c). Moreover, the peak bloom occurred in April instead of May (compare Figs. 12d and
472 12f). This over-growth of *P. minimum* in April consumed a large amount of nutrient, leading to
473 slower growth of *P. minimum* in May even though the temperature in May was more favorable.
474 These results clearly showed that DIP was the dominant nutrient regulating the *P. minimum*
475 blooms, in agreement with previous analysis (e.g., J. Li et al., 2015).

476

477 *3.4 Model sensitivity analysis*

478 Three groups of numerical experiments were conducted to examine how the model
479 results are sensitive to the choice of specific growth rate, initial cell biomass, and the PO_4^{3-} half
480 saturation value.

481 In the control run, the optimal temperature for maximum growth rate T_{opt} was set at 20
482 °C, as a way to reconcile recent observations of Tango et al. (2005) against earlier measurements
483 of Tyler and Seliger (1981) and the data from the in the Mediterranean Sea (Grzebyk and
484 Berland, 1996) (see Figs. 2a and 2b). A model run was conducted using T_{opt}=25 °C, but the
485 model failed to capture the observed *P. minimum* bloom in May and the modelled cell density
486 remained low (Fig. 13a). Moving T_{opt} to 25 °C delayed the peak *P. minimum* growing season
487 until June when the summer "dinoflagellates" group in the RCA model reached its maximum
488 growth rate and dominated the nutrient uptake. Both Tyler and Seliger (1981) and Grzebyk and
489 Berland (1996) suggested salinity dependence in the specific growth rate of *P. minimum*, as
490 shown in Fig. 2c. An empirical curve G_S was fitted to the experiment data and the specific
491 growth rate calculated as the product $G_T * G_S$. A model run was conducted using $G_T * G_S$ and the
492 predicted bloom size at CB3.3C was only marginally smaller than that obtained from the control
493 run (Fig. 13a). This is expected since G_S varies within a range of 40-60% except at very low
494 salinity, but G_T varies over a range of 0.1 - 1 (compares Figs. 2a and 2c). Since G_S reaches a
495 maximum when salinity reaches 25, the *P. minimum* bloom developed in the lower salinity zones
496 (5 – 15) of the mid and upper Bay would have a smaller biomass if G_S is considered.
497 In the second group of numerical experiments, the sensitivity of the results to the initial
498 condition on *P. minimum* biomass was examined. Due to the paucity of observations of *P.*
499 *minimum* during winter, the initial condition of *P. minimum* was constructed by interpolating the
500 data at three monitoring stations using the distribution obtained from the early surveys (Tyler and
501 Seliger, 1978). It is possible that the winter population of *P. minimum* have changed over the
502 past few decades. Model runs designed to test initial conditions were conducted by multiplying
503 the initial condition by factors of 0.5, 1.5, 2.5 and 3.0. As shown in Fig. 13b, there were only

504 moderate (< 20%) differences in the predicted peak biomass among the model runs. This showed
505 that the prediction of *P. minimum* blooms is relatively insensitive to the initial condition as long
506 as a small seed population exists at the beginning of the year. The bloom size was mostly
507 determined by the growth during the spring season (March to May) rather than the overwintering
508 population (see Fig. 13b).

509 In the third group of numerical experiments, the sensitivity of the model to the choice of
510 the half saturation constant for PO_4^{3-} uptake was assessed (Fig. 13c). The predicted bloom size
511 was very sensitive to K_{mp}. In the model run with K_{mp} =1 μM, no *P. minimum* bloom developed
512 since the surface PO_4^{3-} concentration was well below 1 μM in most of the estuary (Figs. 3d1-d4).
513 No bloom of significant size developed in the model run with K_{mp} =0.1 μM, either. In the model
514 run with K_{mp} =0.001 μM, however, a large bloom developed, with the predicted peak cell density
515 twice that of the observed cell density. These sensitivity analyses demonstrated that the control
516 run with K_{mp} =0.03 μM was calibrated well against the observations.

517

518 *3.5 Multi-year model results*

519 To assess interannual variability in model performance, simulations over 10 years (2002-
520 2011) were conducted using the same set of parameter values used as described above for the
521 year 2006. The only changes among the years were through the boundary forcing such as river
522 flow, riverine nutrient loading, winds and air-sea heat fluxes, and offshore sea levels.

523 There were clear year-to-year differences in the bloom magnitude and spatial distribution
524 based on the predicted cell concentrations and comparisons to observed cell densities in May
525 (Fig. 14). During the wet years of 2003-2005 and 2011 (with higher river flow than the long-term
526 average), the bloom spread downstream and occupied a wide area between 37.5 and 39 ^{o}N. In the

two wet years of 2003 and 2005, both the model and data showed not only an extensive bloom area but also high cell density. In comparison, the observations in the wet years of 2004 and 2011 showed that the bloom also shifted downstream but the bloom magnitude was considerably smaller. A weak bloom was also observed in 2010 in a small upper Bay area around 38.7-39.2 ^{o}N. These small blooms were well captured by the model.

During the dry years of 2006, 2008 and 2009, the bloom was limited to the more northern regions (between 38.5 and 39.2 ^{o}N), even though a bloom was still predicted for the Potomac River tributary. Unlike other dry years, the observed bloom in 2007 spanned a wide area between 37.7 and 39.0 ^{o}N, which was reproduced by the model. In all, the general similarity between the predicted and observed bloom distribution and size over 10-years affirms the model's predictive skill.

4. Discussion

Building upon a coupled hydrodynamic-biogeochemical (ROMS-RCA) model, a mechanistic model for *P. minimum* in Chesapeake Bay was developed, ROMS-RCA-*Prorocentrum*. A rhomboid modeling approach was used, adding *P. minimum* to the two other functional phytoplankton groups (winter-spring and summer species) in the previously developed RCA model. Hindcast simulation of 2006 showed that the model reproduced the observed time series of cell density at the monitoring stations, with the bloom occurring in May, and the model realistically located in the mid-to-upper part of the estuary. The goodness of fit of the model was confirmed by the correlation coefficient, r, between the predicted and observed cell density of 0.70, the root-mean-square error of 0.57×10^6 cell L^{-1}, and the mean absolute error of 0.37×10^6 cell L^{-1}. Moreover, skill metrics in predicting the time series of NO_3^- and PO_4^{3-} are comparable

550 with those reported in previous studies (e.g., Fennel et al., 2006; Glibert et al., 2010; Testa et al.,
551 2014; Feng et al., 2015).

552 There have been few mechanistic simulations of the dynamics of a HAB species using a
553 3D coupled hydrodynamic-biogeochemical model with complete nutrient cycling and other
554 phytoplankton groups in eutrophic waters. A similar model for toxic *Karenia mikimotoi* was
555 developed by adding a module for the HAB taxa into to an ecosystem model (the European
556 Regional Seas Ecosystem Model) and applied to blooms in the English Channel (Vanhoutte-
557 Brunier et al., 2008).

558 The ROMS-RCA-*Prorocentrum* model did not consider mixotrophic feeding which has
559 been shown to provide supplemental nutrition for *P. minimum* in Chesapeake Bay, particularly
560 during nutrient starved conditions (Stoecker et al., 1997; Johnson, 2015). Stoecker et al. (1997)
561 observed ingested cryptophytes as orange-fluorescent inclusions (OFI) under an epifluorescent
562 microscope. However, OFI only appeared in <10% of the samples during April and May,
563 although 50% of *P. minimum* contained OFI during the summer. Laboratory experiments by
564 Johnson (2015) showed that a *P. minimum* isolate from Chesapeake Bay ingested cryptophyte
565 prey when in stationary phase and when starved of N or P. It appears that *P. minimum* is a
566 proficient phototroph, and inducible phagotrophy can provide an important additional nutritional
567 source (Glibert et al., 2012; Johnson, 2015). The model skill herein was high without considering
568 mixotrophy. Given that most of blooms appeared in spring (April and May) and mixotrophic
569 feeding occurred most frequently during the nutrient-poor summer condition, it was reasonable
570 not to consider mixotrophy in this first mechanistic model of *Prorocentrum*. However,
571 mixotrophy is an important nutritional strategy for many HAB species, and mechanistic models
572 are being developed (Flynn and Mitra, 2009; Lin et al., 2018), and will be reported elsewhere.

573 Zooplankton (including microzooplankton) are not explicitly modeled in the ROMS-
574 RCA-*Prorocentrum* model. The grazing term on *P. minimum* is represented by a density-
575 dependent mortality term with the grazing coefficient parameterized as a temperature dependent
576 function. It has previously been reported that microzooplankton grazing on *P. minimum* in
577 Chesapeake Bay was highest between the lower oligohaline and mesohaline regions and during
578 the summer months (Johnson et al., 2003).
579
580 This modeling study confirmed 3 general characteristics of these blooms that have been
581 previously described. First, the model confirmed the conceptual understanding of the seasonal
582 progression of *P. minimum* originally proposed by Tyler and Seliger (1978) but added new
583 insights into mechanisms regulating the timing, duration and size of these blooms. Overwintering
584 populations in the southern most of the estuary were transported up-estuary by the estuarine
585 return flow in the bottom layer. Some cells were mixed to the sun-lit surface water through
586 vertical mixing, where they encountered the spring freshet, favorable nutrient and light
587 conditions developed in the middle and upper parts of Chesapeake Bay. Diagnostic analysis of
588 the *P. minimum* equation [Eq. (1)] showed that the timing and duration of *P. minimum* blooms
589 was mostly determined by the temperature-dependent growth function which peaked around 20
590 ^{o}C and decayed exponentially at lower and higher temperatures. Mortality due to grazing and
591 respiration was an order of magnitude smaller and only played a second role in the bloom
592 termination. Blooms were most abundant under conditions of elevated N:P. Model-sensitivity
593 analysis experiments showed that without P limitation, the predicted blooms may occur one
594 month earlier with the peak cell density 2-5 times higher than the observations (Fig. 12).

595 Second, the model reproduced the differences in spatial distribution of *P. minimum*
596 blooms that occurs between wet and dry years. The interannual variability in the river flow was a
597 major driver of the interannual shifts in the bloom distribution, as explored in a habitat model
598 based on the temperature and salinity tolerance of *P. minimum* (M. Li et al., 2020). However, the
599 habitat model failed to explain the observed cell distribution in some years. For example, no
600 blooms were observed during the wet year of 2004, but the habitat model predicted a favorable
601 habitat area spanning a large part of the mid-Bay. On the other hand, the cell density predicted
602 by the mechanistic model was in a good agreement with the observations (Fig. 14), suggesting
603 that factors such as nutrient concentration could be important in controlling the bloom size. A
604 full mechanistic investigation of the interannual variability in *P. minimum* blooms will be
605 reported in a future study.
606 Third, the model – and the numerical model experiments conducted herein – confirm the
607 conceptual model of nutrient relationships with respect to these blooms proposed by Glibert et al.
608 (2012) and crystalizes the importance of variable half saturation constants for PO_4^{3-} in bloom
609 ecology and in the model. Glibert et al. (2012) hypothesized that *P. minimum* blooms may be
610 initiated at N:P levels that are less than Redfield, often stimulated by a ‘‘flush’’ of nutrients or
611 organic materials. Once growth rate increases, bloom biomass is able to increase, often reaching
612 near monospecific proportions at N:P values greater than Redfield. The *P. minimum* cells are
613 able to sustain biomass levels through the ability to transport PO_4^{3-} very efficiently (i.e., high-
614 affinity transporters, represented by low Ks values). Alternatively, at these low PO_4^{3-} conditions,
615 mixotrophic interactions may take on more importance, and this can be explored in future
616 modeling investigations. Thus, while high growth rates may allow blooms to initiate, adaptive
617 physiology is hypothesized to allow blooms to be maintained at less than maximal growth rates

and at non-optimal N:P ratios. The phenomenon of *P. minimum* blooms being sustained at nutrient levels well in excess of classic Redfield proportions (elevated N:P conditions) has also been illustrated in data from the Baltic Sea (Hajdu et al., 2005), the Delaware Inland Bays (Handy et al., 2008), the Neuse River Estuary (Springer et al., 2005), and for the comparable *P. donghainese* species, the East China Sea (J. Li et al., 2009).

In summary, this modeling study has demonstrated how a rhomboid approach can be used to configure a HAB model within an existing biogeochemical model. Although this model was specifically parameterized for Chesapeake Bay and for *P. minimum*, the ROMS-RCA-*Prorocentrum* model herein should be able to be configured for comparable systems since the coupled hydrodynamic-biogeochemical models ROMS-RCA have been applied to a number of shallow-water coastal systems and the modeling framework for *P. minimum* can be readily adapted for other *Prorocentrum* species. This model can also be reparameterized for other HAB species of Chesapeake Bay. Future iterations of this model will consider mixotrophy and climate change effects.

Acknowledgement:

We thank the reviewers for their helpful comments. This work is a result of research funded by the National Oceanic and Atmospheric Administration National Centers for Coastal Ocean Science Competitive Research Program under award NA17NOS4780180 to UMCES. This is ECOHAB contribution number XXX and contribution number YYYY from the University of Maryland Center for Environmental Science.

Model output is available at https://doi.org/10.5281/zenodo.3479428.

References:

641 Allen, J. I., Blackford, J., Holt, J., Proctor, R., Ashworth, M., Siddorn, J., 2001. A highly
642 spatially resolved ecosystem model for the North West European Continental Shelf. Sarsia
643 86(6), 423-440.
644 Anderson, D. M., Burkholder, J. M., Cochlan, W. P., Glibert, P. M., Gobler, C. J., Heil, C. A.,
645 Kudela, R.M., Parsons, M.L., Rensel, J.J., Townsend, D.W., Trainer, V. L., 2008. Harmful
646 algal blooms and eutrophication: examining linkages from selected coastal regions of the
647 United States. Harmful Algae 8(1), 39-53.
648 Anderson, C. R., Siegel, D. A., Kudela, R. M., Brzezinski, M. A., 2009. Empirical models of
649 toxigenic *Pseudo-nitzschia* blooms: potential use as a remote detection tool in the Santa
650 Barbara Channel. Harmful Algae 8(3), 478-492.
651 Anderson, C. R., Sapiano, M. R., Prasad, M. B. K., Long, W., Tango, P. J., Brown, C. W.,
652 Murtugudde, R., 2010. Predicting potentially toxigenic *Pseudo-nitzschia* blooms in the
653 Chesapeake Bay. J. Mar. Syst. 83(3-4), 127-140.
654 Blauw, A. N., Los, F. J., Huisman, J., Peperzak, L., 2010. Nuisance foam events and *Phaeocystis*
655 *globosa* blooms in Dutch coastal waters analyzed with fuzzy logic. J. Mar. Syst. 83(3-4),
656 115-126.
657 Boesch, D. F., Brinsfield, R. B., Magnien, R. E., 2001. Chesapeake bay eutrophication. J.
658 Environ. Qual. 30(2), 303-320.
659 Brady, D. C., Testa, J. M., Di Toro, D. M., Boynton, W. R., Kemp, W. M., 2013. Sediment flux
660 modeling: calibration and application for coastal systems. Estuar. Coastal Shelf Sci. 117,
661 107-124.

662 Brown, C. W., Hood, R. R., Long, W., Jacobs, J., Ramers, D. L., Wazniak, C., Wiggert, J.D.,
663 Wood, R., Xu, J., 2013. Ecological forecasting in Chesapeake Bay: using a mechanistic–
664 empirical modeling approach. J. Mar. Syst. 125, 113-125.
665 Brush, G. S., 2009. Historical land use, nitrogen, and coastal eutrophication: A paleoecological
666 perspective. Estuar. Coasts 32(1), 18-28.
667 Cembella, A. D., Antia, N. J., Harrison, P. J., Rhee, G. Y., 1984. The utilization of inorganic and
668 organic phosphorous compounds as nutrients by eukaryotic microalgae: a multidisciplinary
669 perspective: part 2. CRC Crit. Rev. Microbiol. 11(1), 13-81.
670 Dam, H. G., Colin, S. P., 2005. *Prorocentrum minimum* (clone Exuv) is nutritionally insufficient,
671 but not toxic to the copepod *Acartia tonsa*. Harmful Algae 4(3), 575-584.
672 DiToro, D. M., Allen, H. E., Bergman, H. L., Meyer, J. S., Paquin, P. R., Santore, R. C., 2001.
673 Biotic ligand model of the acute toxicity of metals. 1. Technical basis. Environ. Toxicol.
674 Chem. 20(10), 2383-2396.
675 Egbert, G. D., Erofeeva, S. Y., 2002. Efficient inverse modeling of barotropic ocean tides. J.
676 Atmos. Ocean. Technol. 19(2), 183-204.
677 Fennel, K., Wilkin, J., Levin, J., Moisan, J., O'Reilly, J., Haidvogel, D., 2006. Nitrogen cycling
678 in the Middle Atlantic Bight: Results from a three-dimensional model and implications for
679 the North Atlantic nitrogen budget. Global Biogeochem. Cy. 20(3).
680 Feng, Y., Friedrichs, M. A., Wilkin, J., Tian, H., Yang, Q., Hofmann, E. E., Wiggert, J.D., Hood,
681 R. R., 2015. Chesapeake Bay nitrogen fluxes derived from a land-estuarine ocean
682 biogeochemical modeling system: Model description, evaluation, and nitrogen budgets. J.
683 Geophys. Res. Biogeo. 120(8), 1666-1695.

684 Filippino, K. C., Mulholland, M. R., Bernhardt, P. W., 2011. Nitrogen uptake and primary
685 productivity rates in the Mid-Atlantic Bight (MAB). Estuar. Coast. Shelf Sci. 91(1), 13-23.
686 Fisher, T. R., Peele, E. R., Ammerman, J. W., Harding Jr, L. W., 1992. Nutrient limitation of
687 phytoplankton in Chesapeake Bay. Mar. Ecol. Prog. Ser. 51-63.
688 Fisher, T. R., Hagy, J. I. D., Boynton, W. R., Williams, M. R., 2006. Cultural eutrophication in
689 the Choptank and Patuxent estuaries of Chesapeake Bay. Limnol. Oceanogr. 51(part2), 435-
690 447.
691 Flynn, K. J., McGillicuddy, D. J., 2018. Modeling marine harmful algal blooms: Current status
692 and future prospects. Harmful Algal Blooms: A Compendium Desk Reference, 115-134.
693 Flynn, K. J., Mitra, A., 2009. Building the "perfect beast": modelling mixotrophic plankton. J.
694 Plankton Res. 31(9), 965-992.
695 Franks, P. J., 2018. Recent advances in modelling of harmful algal blooms. In Global Ecology
696 and Oceanography of Harmful Algal Blooms (pp. 359-377). Springer, Cham.
697 Garcia, H. E., Locarnini, R. A., Boyer, T. P., Antonov, J. I., Baranova, O. K., Zweng, M. M.,
698 Reagan, J. R., Johnson, D. R., Mishonov, A. V., Levitus, S., 2013. World ocean atlas 2013.
699 Volume 4, Dissolved inorganic nutrients (phosphate, nitrate, silicate).
700 Giddings, S. N., MacCready, P., Hickey, B. M., Banas, N. S., Davis, K. A., Siedlecki, S. A.,
701 Trainer, V. L., Kudela, R. M., Pelland, N. A., Connolly, T. P., 2014. Hindcasts of potential
702 harmful algal bloom transport pathways on the Pacific Northwest coast. J. Geophys. Res.
703 Oceans 119(4), pp.2439-2461.
704 Gillibrand, P. A., Siemering, B., Miller, P. I., Davidson, K., 2016. Individual-based modelling of
705 the development and transport of a *Karenia mikimotoi* bloom on the North-west European
706 continental shelf. Harmful Algae 53, 118-134.

Glibert, P. M., Allen, J. I., Bouwman, A. F., Brown, C. W., Flynn, K. J., Lewitus, A. J., Madden, C. J., 2010. Modeling of HABs and eutrophication: status, advances, challenges. J. Mar. Syst. 83(3-4), 262-275.

Glibert, P.M., A.H.W. Beausen, A.F. Bouwman, J.M. Burkholder, K.J. Flynn, C.A. Heil, M. Li, C-H. Lin, C.J. Madden, A. Mitra, W. Nardon, G. Silsbe, Y. Song, F. Zhang. (2020). Multifaceted climate change and nutrient effects on harmful algae require multifaceted models. Chapter 12 in Climate change and marine and freshwater toxins. Edited by Botana LM, C. Louzao and N. Vilariño), 2nd edition. DeGruyter Publishers. ISBN 978-3-11-062292-8. pp. 473-518. doi: 10.1515/9783110625738-012.

Glibert, P. M., Burkholder, J. M., Kana, T. M., 2012. Recent insights about relationships between nutrient availability, forms, and stoichiometry, and the distribution, ecophysiology, and food web effects of pelagic and benthic *Prorocentrum* species. Harmful Algae 14, 231-259.

Glibert, P. M., Magnien, R., Lomas, M. W., Alexander, J., Tan, C., Haramoto, E., Trice, M., Kana, T.M., 2001. Harmful algal blooms in the Chesapeake and coastal bays of Maryland, USA: comparison of 1997, 1998, and 1999 events. Estuaries 24(6), 875-883.

Glibert, P. M., Mayorga, E., Seitzinger, S., 2008. *Prorocentrum minimum* tracks anthropogenic nitrogen and phosphorus inputs on a global basis: application of spatially explicit nutrient export models. Harmful Algae 8(1), 33-38.

Glibert, P. M., Seitzinger, S., Heil, C. A., Burkholder, J. M., Parrow, M. W., Codispoti, L. A., Kelly, V., 2005. Eutrophication. Oceanography 18(2), 198.

Gómez, F., 2005. A list of free-living dinoflagellate species in the world's oceans. Acta Bot. Croat. 64(1), 129-212.

730 Grzebyk, D., Berland, B., 1996. Influences of temperature, salinity and irradiance on growth of
731 *Prorocentrum minimum* (Dinophyceae) from the Mediterranean Sea. J. Plankton
732 Res. 18(10), 1837-1849.
733 Hagy, J. D., Boynton, W. R., Keefe, C. W., Wood, K. V., 2004. Hypoxia in Chesapeake Bay,
734 1950–2001: long-term change in relation to nutrient loading and river flow. Estuaries 27(4),
735 634-658.
736 Haidvogel, D. B., Arango, H., Budgell, W. P., Cornuelle, B. D., Curchitser, E., Di Lorenzo,
737 E., Fennel, K., Geyer, W.R., Hermann, A.J., Lanerolle, L. Levin, J., 2008. Ocean
738 forecasting in terrain-following coordinates: Formulation and skill assessment of the
739 Regional Ocean Modeling System. J. Comput. Phys. 227(7), 3595-3624.
740 Hajdu, S., Pertola, S., Kuosa, H., 2005. *Prorocentrum minimum* (Dinophyceae) in the Baltic Sea:
741 morphology, occurrence—a review. Harmful Algae 4(3), 471-480.
742 Handy, S. M., Demir, E., Hutchins, D. A., Portune, K. J., Whereat, E. B., Hare, C. E., Rose, J.M.,
743 Warner, M., Farestad, M., Farestad, M., Cary, S.C. Coyne, K. J., 2008. Using quantitative
744 real-time PCR to study competition and community dynamics among Delaware Inland Bays
745 harmful algae in field and laboratory studies. Harmful Algae 7(5), 599-613.
746 Harding Jr, L. W., Adolf, J. E., Mallonee, M. E., Miller, W. D., Gallegos, C. L., Perry, E. S.,
747 Johnson, J. M., Sellner, K. G., Paerl, H.W., 2015. Climate effects on phytoplankton floral
748 composition in Chesapeake Bay. Estuar. Coast. Shelf Sci. 162, pp.53-68.
749 Harding Jr, L. W., Mallonee, M. E., Perry, E. S., 2002. Toward a predictive understanding of
750 primary productivity in a temperate, partially stratified estuary. Estuar. Coast. Shelf Sci.
751 55(3), 437-463.

752 Harding, L. W., Gallegos, C. L., Perry, E. S., Miller, W. D., Adolf, J. E., Mallonee, M. E., Paerl,
753 H. W., 2016. Long-term trends of nutrients and phytoplankton in Chesapeake Bay. Estuar.
754 Coasts 39(3), 664-681.
755 He, R., McGillicuddy Jr, D. J., Keafer, B. A., Anderson, D. M., 2008. Historic 2005 toxic bloom
756 of *Alexandrium fundyense* in the western Gulf of Maine: 2. Coupled biophysical numerical
757 modeling. J. Geophys. Res. Oceans 113(C7).
758 Heil, C. A., 2005. Influence of humic, fulvic and hydrophilic acids on the growth, photosynthesis
759 and respiration of the dinoflagellate *Prorocentrum minimum* (Pavillard) Schiller. Harmful
760 Algae 4(3), 603-618.
761 Heil, C. A., Glibert, P. M., Fan, C., 2005. *Prorocentrum minimum* (Pavillard) Schiller: a review
762 of a harmful algal bloom species of growing worldwide importance. Harmful Algae 4(3),
763 449-470.
764 Isleib, R. R., Fitzpatrick, J. J., Mueller, J., 2007. The development of a nitrogen control plan for a
765 highly urbanized tidal embayment. Proceedings of the Water Environment
766 Federation 2007(5), 296-320.
767 Jiang, J., Shen, A., Wang, H., Yuan, S., 2019. Regulation of phosphate uptake kinetics in the
768 bloom-forming dinoflagellates *Prorocentrum donghaiense* with emphasis on two-stage
769 dynamic process. J. Theor. Biol. 463, 12-21.
770 Johnson, M. D. (2015). Inducible mixotrophy in the dinoflagellate *Prorocentrum minimum*. J.
771 Eukaryot. Microbiol. 62(4), 431-443.
772 Johnson, M. D., Rome, M., Stoecker, D. K., 2003. Microzooplankton grazing on *Prorocentrum*
773 *minimum* and *Karlodinium micrum* in Chesapeake Bay. Limnol. Oceanogr. 48(1), 238-248.
774 Jolliff, J. K., Kindle, J. C., Shu, I., 2009. Summary diagrams for coupled hydrodynamic-

775 ecosystem model skill assessment. J. Mar. Syst. 76, 64-82.
776 Kemp, W. M., Boynton, W. R., Adolf, J. E., Boesch, D. F., Boicourt, W. C., Brush, G., Cornwell,
777 J. C., Fisher, T. R., Glibert, P. M., Hagy, J. D., Harding, L. W., 2005. Eutrophication of
778 Chesapeake Bay: historical trends and ecological interactions. Mar. Ecol. Prog. Ser. 303, 1-
779 29.
780 Kemp, W. M., Testa, J. M., Conley, D. J., Gilbert, D., Hagy, J. D., 2009. Temporal responses of
781 coastal hypoxia to nutrient loading and physical controls. Biogeosciences 6(12), 2985-3008.
782 Li, J., Glibert, P. M., Zhou, M., Lu, S., Lu, D., 2009. Relationships between nitrogen and
783 phosphorus forms and ratios and the development of dinoflagellate blooms in the East
784 China Sea. Mar. Ecol. Prog. Ser. 383, 11-26.
785 Li, J., Glibert, P. M., Gao, Y., 2015. Temporal and spatial changes in Chesapeake Bay water
786 quality and relationships to *Prorocentrum minimum*, *Karlodinium veneficum*, and
787 CyanoHAB events, 1991–2008. Harmful Algae 42, 1-14.
788 Li, M., Lee, Y. J., Testa, J. M., Li, Y., Ni, W., Kemp, W. M., Di Toro, D. M., 2016. What drives
789 interannual variability of hypoxia in Chesapeake Bay: Climate forcing versus nutrient
790 loading?. Geophys. Res. Lett. 43(5), 2127-2134.
791 Li, M., Ni, W., Zhang, F., Glibert, P. M., Lin, C.-H., 2020. Climate-induced interannual
792 variability and projected change of two harmful algal bloom taxa in Chesapeake Bay, USA.
793 Sci. Total Environ. 744, 140947.
794 Li, M., Zhong, L., Harding, L. W., 2009. Sensitivity of plankton biomass and productivity to
795 variations in physical forcing and biological parameters in Chesapeake Bay. J. Mar. Res.
796 67(5), 667-700.

797 Li, M., Zhong, L., Boicourt, W. C., 2005. Simulations of Chesapeake Bay estuary: Sensitivity to
798 turbulence mixing parameterizations and comparison with observations. J. Geophys. Res.
799 Oceans 110(C12).
800 Li, M., Zhong, L., Boicourt, W. C., Zhang, S., Zhang, D. L., 2006. Hurricane-induced storm
801 surges, currents and destratification in a semi-enclosed bay. Geophys. Res. Lett. 33(2).
802 Li, Y., He, R., Manning, J. P., 2014. Coastal connectivity in the Gulf of Maine in spring and
803 summer of 2004–2009. Deep Sea Res. Part II Top. Stud. Oceanogr. 103, 199-209.
804 Lin, C. H., Flynn, K. J., Mitra, A., Glibert, P. M., 2018. Simulating effects of variable
805 stoichiometry and temperature on mixotrophy in the harmful dinoflagellate *Karlodinium*
806 *veneficum*. Front. Mar. Sci. 5, 320.
807 Lin, S., Litaker, R. W., Sunda, W. G., 2016. Phosphorus physiological ecology and molecular
808 mechanisms in marine phytoplankton. J. Appl. Phycol. 52(1), 10-36.
809 Lomas, M. W., Glibert, P. M., 1999. Interactions between NH_4^+ and NO_3^- uptake and
810 assimilation: comparison of diatoms and dinoflagellates at several growth
811 temperatures. Mar. Biol. 133(3), 541-551.
812 McGillicuddy Jr, D. J., 2010. Models of harmful algal blooms: conceptual, empirical, and
813 numerical approaches. J. Mar. Syst. 83(3-4), 105.
814 McGillicuddy, D. J., Townsend, D. W., He, R., Keafer, B. A., Kleindinst, J. L., Li, Y., Manning,
815 J. P., Mountain, D. G., Thomas, M. A. and Anderson, D. M., 2011. Suppression of the 2010
816 *Alexandrium fundyense* bloom by changes in physical, biological, and chemical properties
817 of the Gulf of Maine. Limnol. Oceanogr. 56(6), pp. 2411-2426.
818 Mitra, A., Davis, C., 2010. Defining the “to” in end-to-end models. Prog. Oceanogr. 84(1-2), 39-
819 42.

820 Ni, W., Li, M., Testa, J. M., 2020. Discerning effects of warming, sea level rise and nutrient
821 management on long-term hypoxia trends in Chesapeake Bay. Sci. Total Environ. 737,
822 139717.
823 Obenour, D. R., Gronewold, A. D., Stow, C. A., Scavia, D., 2014. Using a Bayesian hierarchical
824 model to improve Lake Erie cyanobacteria bloom forecasts. Water Resour. Res. 50(10),
825 7847-7860.
826 Ou, L., Wang, D., Huang, B., Hong, H., Qi, Y., Lu, S., 2008. Comparative study of phosphorus
827 strategies of three typical harmful algae in Chinese coastal waters. J. Plankton Res. 30(9),
828 1007-1017.
829 Pertola, S., Kuosa, H., Olsonen, R., 2005. Is the invasion of *Prorocentrum minimum*
830 (Dinophyceae) related to the nitrogen enrichment of the Baltic Sea? Harmful Algae 4(3),
831 481-492.
832 Pinto, L., Mateus, M., Silva, A., 2016. Modeling the transport pathways of harmful algal blooms
833 in the Iberian coast. Harmful Algae 53, 8-16.
834 Raine, R., McDermott, G., Silke, J., Lyons, K., Nolan, G., Cusack, C., 2010. A simple short
835 range model for the prediction of harmful algal events in the bays of southwestern Ireland. J.
836 Mar. Syst. 83(3-4), 150-157.
837 Ralston, D. K., Moore, S. K., 2020. Modeling harmful algal blooms in a changing climate.
838 Harmful Algae 91, 101729.
839 Shchepetkin, A. F., McWilliams, J. C., 2005. The regional oceanic modeling system (ROMS): a
840 split-explicit, free-surface, topography-following-coordinate oceanic model. Ocean
841 Model. 9(4), 347-404.

842 Shchepetkin, A. F., McWilliams, J. C., 2009a. Computational kernel algorithms for fine-scale,
843 multiprocess, longtime oceanic simulations. In Handbook of Numerical Analysis (Vol. 14,
844 pp. 121-183). Elsevier.
845 Shchepetkin, A. F., McWilliams, J. C., 2009b. Correction and commentary for "Ocean
846 forecasting in terrain-following coordinates: Formulation and skill assessment of the
847 regional ocean modeling system" by Haidvogel et al., J. Comp. Phys. 227, pp. 3595–3624. J.
848 Comp. Phys. 228(24), 8985-9000.
849 Smayda, T. J., 1996. Dinoflagellate bloom cycles: what is the role of cellular growth rate and
850 bacteria? Harmful Toxic Algal Bloom. 331-334.
851 Sohn, M. H., Lim, S., Seo, K. W., Lee, S. J., 2013. Effect of ambient medium viscosity on the
852 motility and flagella motion of *Prorocentrum minimum* (Dinophyceae). J. Plankton Res.
853 35(6), 1294-1304.
854 Springer, J. J., Burkholder, J. M., Glibert, P. M., Reed, R. E., 2005. Use of a real-time remote
855 monitoring network (RTRM) and shipborne sampling to characterize a dinoflagellate bloom
856 in the Neuse Estuary, North Carolina, USA. Harmful Algae 4(3), 533-551.
857 Stock, C. A., McGillicuddy Jr, D. J., Solow, A. R., Anderson, D. M., 2005. Evaluating
858 hypotheses for the initiation and development of *Alexandrium fundyense* blooms in the
859 western Gulf of Maine using a coupled physical–biological model. Deep Sea Res. Part II
860 Top. Stud. Oceanogr. 52(19-21), 2715-2744.
861 Stoecker, D. K., Li, A., Coats, D. W., Gustafson, D. E., Nannen, M. K., 1997. Mixotrophy in the
862 dinoflagellate *Prorocentrum minimum*. Mar. Ecol. Prog. Ser. 152, 1-12.

Stumpf, R.P., Tomlinson, M.C., Calkins, J.A., Kirkpatrick, B., Fisher, K., Nierenberg, K., Currier, R., Wynne, T.T., 2009. Skill assessment for an operational algal bloom forecast system. J. Mar. Syst., 76(1-2), 151-161.

Tango, P. J., Magnien, R., Butler, W., Luckett, C., Luckenbach, M., Lacouture, R., Poukish, C., 2005. Impacts and potential effects due to *Prorocentrum minimum* blooms in Chesapeake Bay. Harmful Algae 4(3), 525-531.

Taylor, K. E., 2001. Summarizing multiple aspects of model performance in a single diagram. J. Geophys. Res. Atmos. 106**,** 7183-7192.

Taylor, G. T., Gobler, C. J., Sañudo-Wilhelmy, S. A., 2006. Speciation and concentrations of dissolved nitrogen as determinants of brown tide *Aureococcus anophagefferens* bloom initiation. Mar. Ecol. Prog. Ser. 312, 67-83.

Testa, J. M., Li, Y., Lee, Y. J., Li, M., Brady, D. C., Di Toro, D. M., Kemp, M., Fitzpatrick, J. J., 2014. Quantifying the effects of nutrient loading on dissolved O2 cycling and hypoxia in Chesapeake Bay using a coupled hydrodynamic–biogeochemical model. J. Mar. Syst. 139, 139-158.

Testa, J.M., Y. Li, Y.J. Lee, M. Li, D.C. Brady, D.M. DiToro, and W.M. Kemp. (2017). Modeling physical and biogeochemical controls on dissolved oxygen in Chesapeake Bay: lessons learned from simple and complex approaches. Chapter 6 in in *Modeling Coastal Hypoxia - Numerical Simulations of Patterns, Controls and Effects of Dissolved Oxygen Dynamics*, edited by D. Justic, K. Rose, R. Hetland, and K. Fennel. Springer International Publishing AG, Switzerland, 95-118, doi: 10.1007/978-3-310-54571-4_5.

884 Tyler, M. A., Seliger, H. H., 1978. Annual subsurface transport of a red tide dinoflagellate to its
885 bloom area: Water circulation patterns and organism distributions in the Chesapeake Bay
886 1. Limnol. Oceanogr. 23(2), 227-246.
887 Tyler, M. A., Seliger, H. H., 1981. Selection for a red tide organism: Physiological responses to
888 the physical environment 1, 2. Limnol. Oceanogr. 26(2), 310-324.
889 Vanhoutte-Brunier, A., Fernand, L., Ménesguen, A., Lyons, S., Gohin, F., Cugier, P., 2008.
890 Modelling the *Karenia mikimotoi* bloom that occurred in the western English Channel
891 during summer 2003. Ecol Modell. 210(4), 351-376.
892 Warner, J. C., Geyer, W. R., Lerczak, J. A., 2005. Numerical modeling of an estuary: A
893 comprehensive skill assessment. J. Geophys. Res. Oceans 110(C5).
894 Xu, H., Min, G. S., Choi, J. K., Zhu, M., Jiang, Y., Al-Rasheid, K. A., 2010. Temporal
895 population dynamics of dinoflagellate *Prorocentrum minimum* in a semi-enclosed
896 mariculture pond and its relationship to environmental factors and protozoan grazers. Chin.
897 J. Oceanol. Limn. 28(1), 75-81.
898 DeYoung, B., Heath, M., Werner, F., Chai, F., Megrey, B., Monfray, P., 2004. Challenges of
899 modeling ocean basin ecosystems. Science 304(5676), 1463-1466.
900 Xie, X., Li, M., 2018. Effects of wind straining on estuarine stratification: A combined
901 observational and modeling study. J. Geophys. Res. Oceans 123(4), 2363-2380.
902 Xie, X., Li, M., Ni, W., 2018. Roles of Wind-Driven Currents and Surface Waves in Sediment
903 Resuspension and Transport During a Tropical Storm. J. Geophys. Res. Oceans 123(11),
904 8638-8654.
905 Zhang, H., Li, S., 2010. Effects of physical and biochemical processes on the dissolved oxygen
906 budget for the Pearl River Estuary during summer. J. Mar. Syst. 79(1-2), 65-88.

907 Zhong, L., Li, M., 2006. Tidal energy fluxes and dissipation in the Chesapeake Bay. Cont. Shelf
908 Res. 26(6), 752-770.
909 Zimmerman, A. R., Canuel, E. A., 2002. Sediment geochemical records of eutrophication in the
910 mesohaline Chesapeake Bay. Limnol. Oceanogr. 47(4), 1084-1093.
911

912 **Figure Captions**

913 Figure 1. (a) The horizontal curvilinear coordinate system for ROMS-RCA model, every third
914 grid line is plotted in both along- and cross-bay directions. The red dashed line marks the
915 location of the along-channel section and the numbers indicate the distance to the mouth of the
916 Bay. (b) The bathymetry of Chesapeake Bay. The black squares and open circles mark the
917 location of observational sites used for model validation.

918 Figure 2. (a) Growth rate of *P. minimum* as a function of temperature. Blue open circles
919 represent data from Tyler and Seliger (1981), red open circles represent data from Grzebyk and
920 Berland (1996), pink triangles represent data from Lomas and Glibert (1999), and dashed black
921 line represents the growth curve adopted by the RCA model. All growth rates in (a) were
922 normalized by the corresponding maximum specific growth rate. (b) *P. minimum* habitat
923 suggesting favorable salinity and temperature conditions for bloom (filled black squares) in
924 Chesapeake Bay (Modified from Tango et al. 2005). (c) Growth rate of *P. minimum* as a function
925 of salinity. Blue open circles represent data from Tyler and Seliger (1981), red open circles
926 represent data from Grzebyk and Berland (1996). Both growth rates were normalized by the
927 corresponding mean growth rate. Dashed black line is the fitted curve which was used in the
928 salinity sensitivity experiment.

929 Figure 3. (a) Observed time series of daily freshwater discharge (blue) and monthly total
930 nitrogen (green) and phosphate (pink) load from Susquehanna River for year 2006. (b-i)
931 Comparison between the predicted (red) and observed (black) nutrient and Chl *a* concentrations
932 at stations along the main axis of Chesapeake Bay for year 2006 (left to right on the horizontal
933 axis: upstream to downstream). Column (b)-(e) are for surface water and Column (f)-(i) are for

934 bottom water. Rows 1 to 4 are for spring to winter seasons. Error bar represents standard
935 deviations from 3-month seasonal averages.

936 Figure 4. Taylor (left) and Target (right) diagrams for comparing the predicted and observed
937 surface NO_3^- (top) and PO_4^{3-} (bottom) concentrations at several monitoring stations in
938 Chesapeake Bay.

939 Figure 5. Comparison between the predicted (red) and observed (black) *P. minimum* cell
940 concentration at 3 main stem stations (due to data availability) and 2 tributary stations in year
941 2006. The black open circles represent the observational monthly mean cell concentration, and
942 the thick red line and red dots represent the model-predicted monthly and daily mean cell
943 concentration, respectively.

944 Figure 6. Predicted monthly-mean *P. minimum* cell concentration in the surface water of
945 Chesapeake Bay in 2006.

946 Figure 7. Predicted monthly-mean *P. minimum* cell concentration in the along-channel section.
947 The vectors are monthly-mean subtidal flow. Please note the range of color bar in (d)-(f) is
948 different from others.

949 Figure 8. Snapshots of *P. minimum* cell concentration in the along-channel section during the
950 development and decline of the bloom in 2006. The vectors are subtidal flows that filtered out
951 tidal signals using 40-hour butterworth filter.

952 Figure 9. Monthly-averaged concentration of (a-c) NO_3^-+NH_4^+, (d-f) PO_4^{3-}, and (g-i) *P. minimum*
953 in the along-channel section during spring months. Filled color contours in (a)-(f) are in
954 logarithm scale.

Figure 10. Along-channel distribution of (a) DIN limitation, (b) DIP limitation, (c) specific growth rate with black contour lines showing water temperature, (d) light limitation, (e) growth rate (considering temperature, nutrient, and light effects), and (f) *P. minimum* cell concentration during May.

Figure 11. Time series of the predicted (a) water temperature, (b) specific growth rate, (c) nutrient limitation, (d) light limitation, (e) biomass growth rate (G*$proro$), (f) grazing loss rate (R_{gz}*$proro^2$), (g) respiration loss rate (R_{res}*$proro$), and (h) cell concentration of *P. minimum* in the surface water of CB4.1C. The shaded yellow area in (a)-(b) mark the period when temperature is optimal for *P. minimum* growth. The dashed red lines in (e)-(g) indicate when biomass growth rate, grazing loss rate, and respiration loss rate reach the peak value, respectively.

Figure 12. Surface distribution of the annual peak *P. minimum* cell concentration from (a) control run, and experiments with (b) no DIN and (c) no DIP limitation on algal growth. (d)-(f) Monthly maximum concentration of *P. minimum* in Chesapeake Bay surface water from the same 3 runs. The red lines represent the median value and the blue boxes spans the interquartile range.

Figure 13. Time series of surface *P. minimum* concentration at CB 3.3C from different sensitivity experiments. (a) Results from salinity effect and optimal temperature experiments. The pink line represents result from experiment with salinity effect and the green line represents result from experiment with optimal temperature at 25^{o}C. (b) Results from initial condition experiments. Initial *P. minimum* concentration was scaled by 0.5, 1.5, 2, and 3 in each experiment. (c) Results from the half saturation coefficient K_{mp} experiments. K_{mp} = 0.001 μM (green), 0.1 μM (yellow), and 1 μM (red) was tested.

976 Figure 14. Surface *P. minimum* concentration averaged over May for each year between 2002-
977 2011. Filled color contours are results from model predictions and filled color circles represent
978 observations.

979

980 **Table Captions**

981 Table 1. Values of the parameters used in the *P. minimum* model.

982 Table 2. Correlation coefficient (r), root mean square error (RMSE), skill, mean absolute error,
983 and mean error for model-data comparison of *P. minimum* cell density for 2006. Both model and
984 observational data were monthly averaged for these comparisons.

985

986

987

(a)

(b)

300
250
200
150
100
50
0

CB2.2
CB3.1
CB3.3C
CB4.1C
CB4.2C
CB4.3C
ET5.2
LE2.2
CB5.2
CB6.1

39°N
38°N
37°N
77°W
76°W

Latitude
Longitude

20
18
16
14
12
10
8
6
4
2
0
Depth [m]

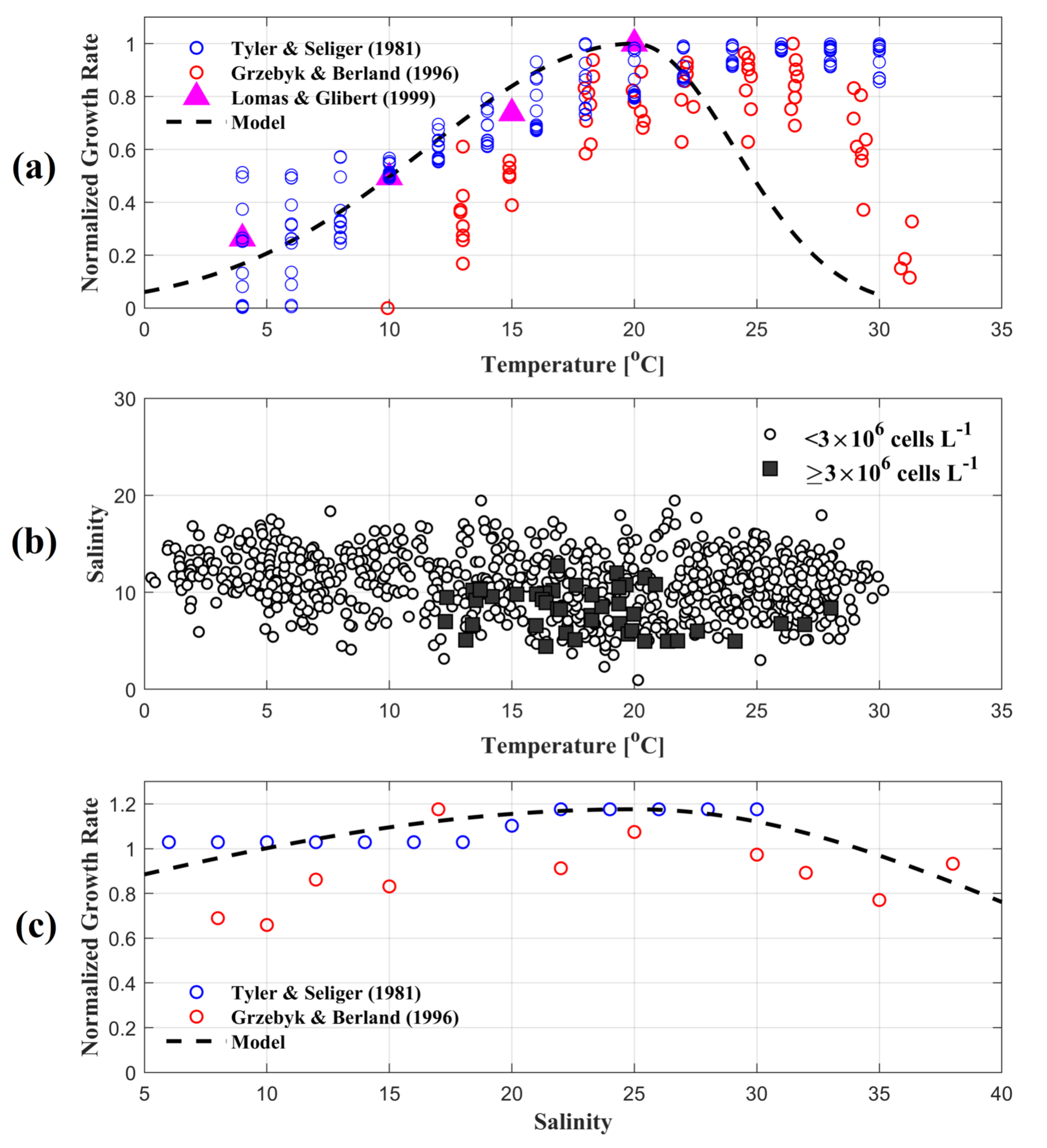
(a)
Normalized Growth Rate
Tyler & Seliger (1981)
Grzebyk & Berland (1996)
Lomas & Glibert (1999)
Model
Temperature [°C]
(b)
Salinity
<3×10^6 cells L^-1
≥3×10^6 cells L^-1
Temperature [°C]
(c)
Normalized Growth Rate
Tyler & Seliger (1981)
Grzebyk & Berland (1996)
Model
Salinity

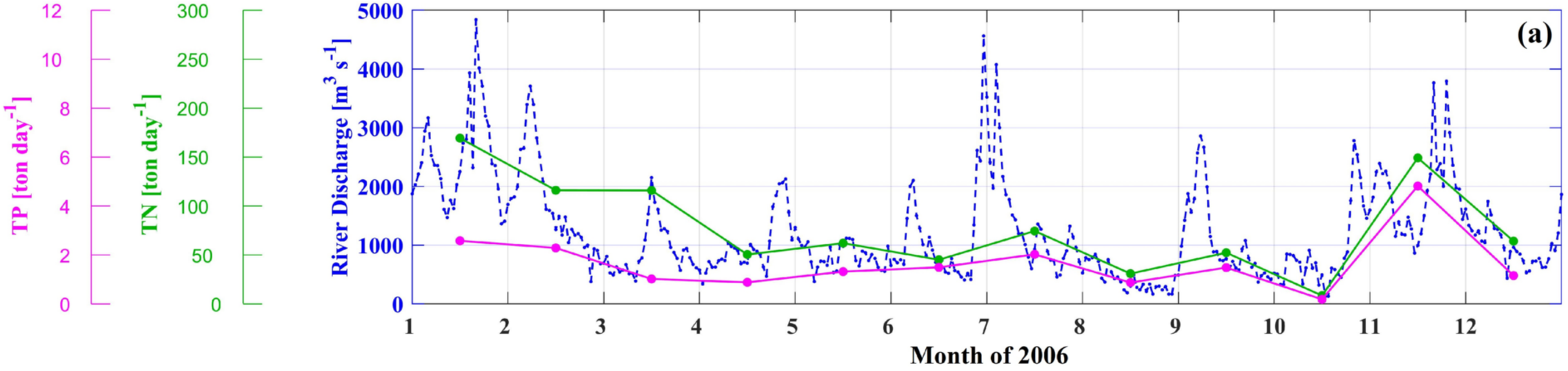
(a)
TP [ton day^{-1}]
TN [ton day^{-1}]
River Discharge [m^3 s^{-1}]
Month of 2006

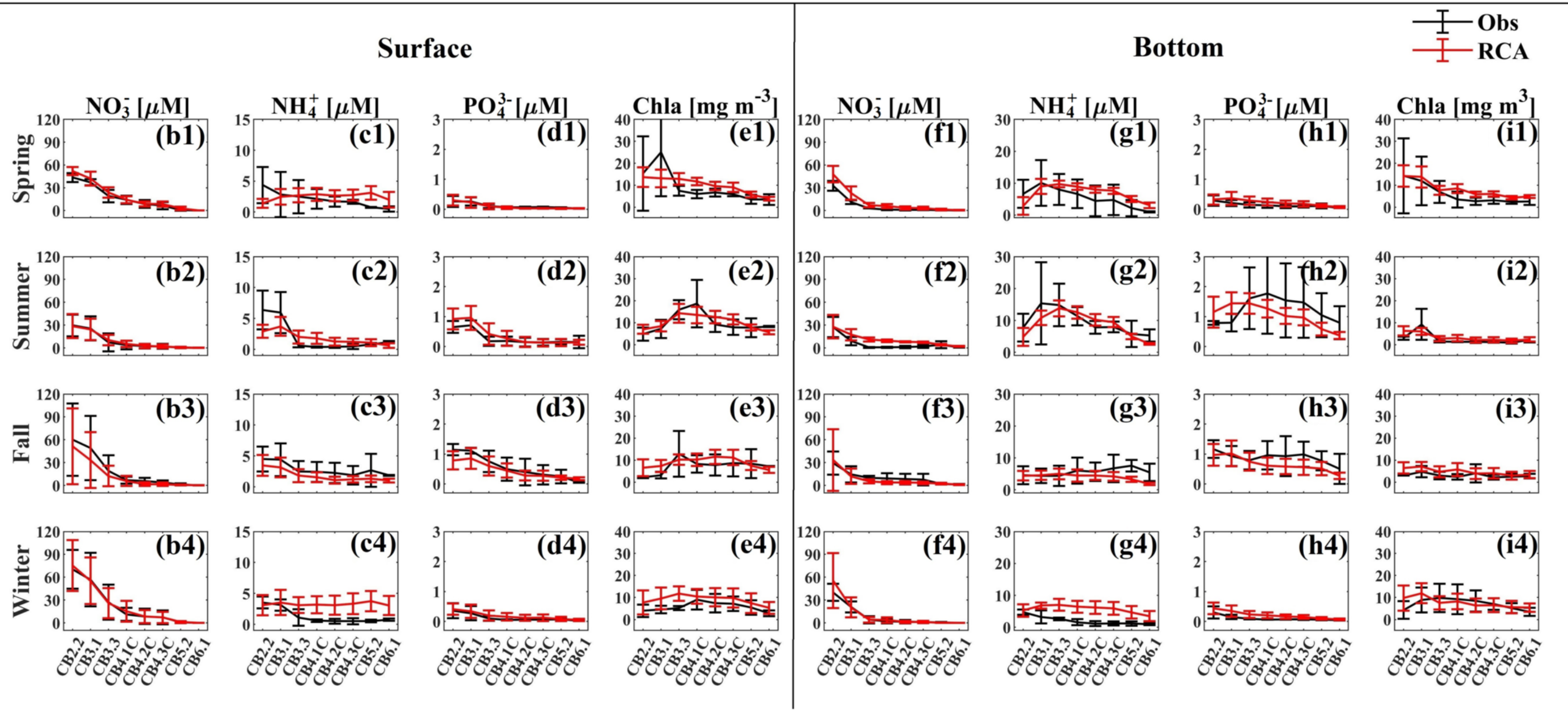
Surface
Bottom
Obs
RCA
NO$_3^-$ [μM]
NH$_4^+$ [μM]
PO$_4^{3-}$ [μM]
Chla [mg m^{-3}]
Spring
Summer
Fall
Winter
(b1)
(c1)
(d1)
(e1)
(f1)
(g1)
(h1)
(i1)
(b2)
(c2)
(d2)
(e2)
(f2)
(g2)
(h2)
(i2)
(b3)
(c3)
(d3)
(e3)
(f3)
(g3)
(h3)
(i3)
(b4)
(c4)
(d4)
(e4)
(f4)
(g4)
(h4)
(i4)
CB2.2
CB3.1
CB3.3
CB4.1C
CB4.2C
CB4.3C
CB5.2
CB6.1

NO_3^-

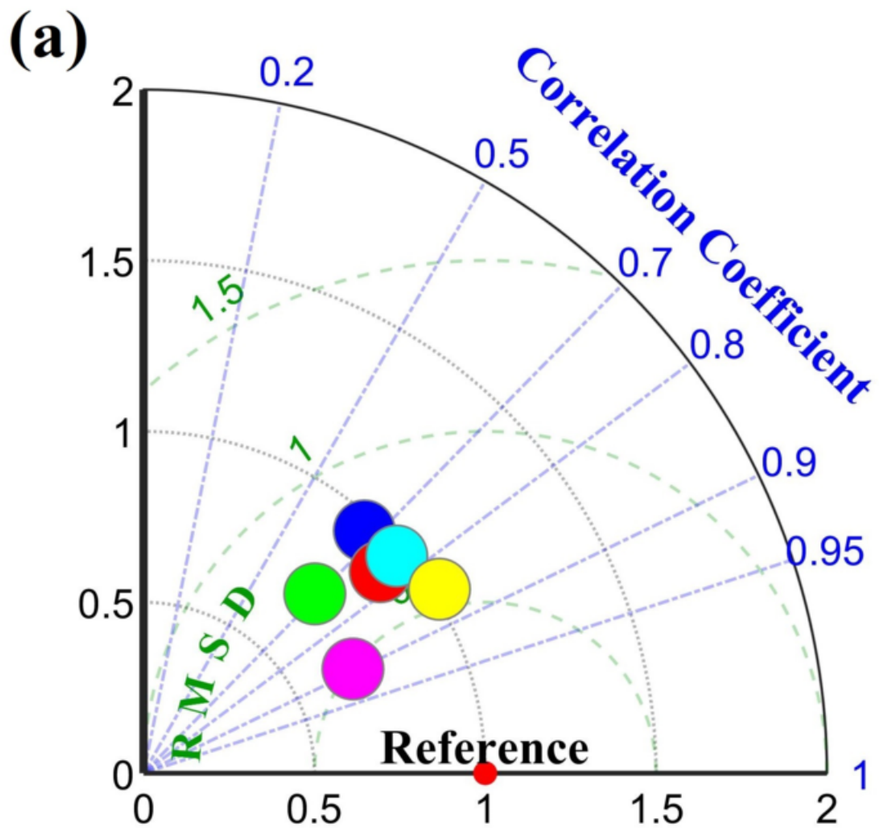
(a)
Correlation Coefficient
0.2
0.5
0.7
0.8
0.9
0.95
1
1.5
RMSD
Reference
0
0.5
1
1.5
2

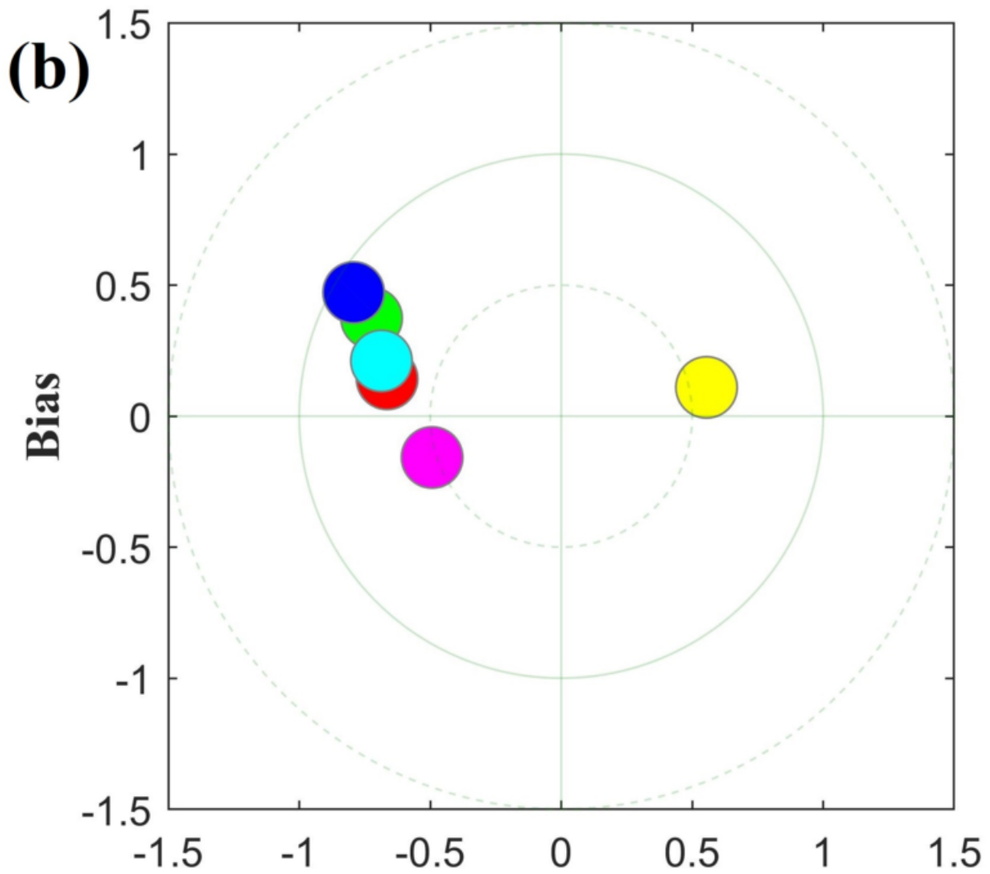
(b)
Bias
1.5
1
0.5
0
-0.5
-1
-1.5
CB3.1
CB3.3C
CB4.1C
CB4.2C
CB4.3C
CB5.2

PO_4^{3-}

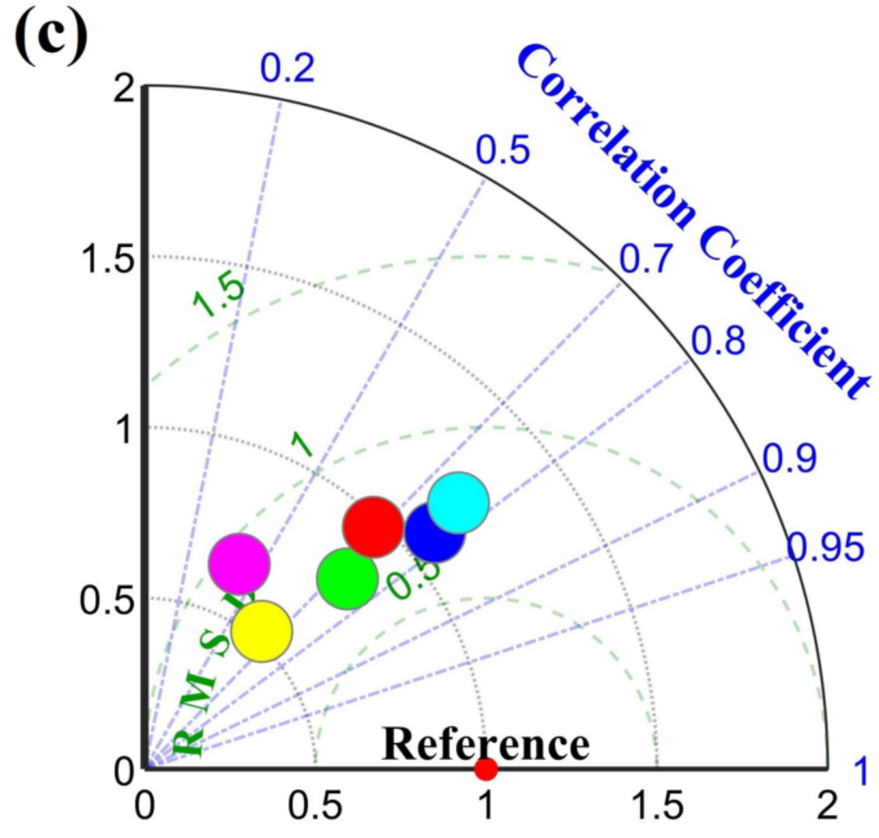
(c)
Correlation Coefficient
0.2
0.5
0.7
0.8
0.9
0.95
1
1.5
0.5
RMSD
Reference
0
0.5
1
1.5
2
Normalized standard deviation

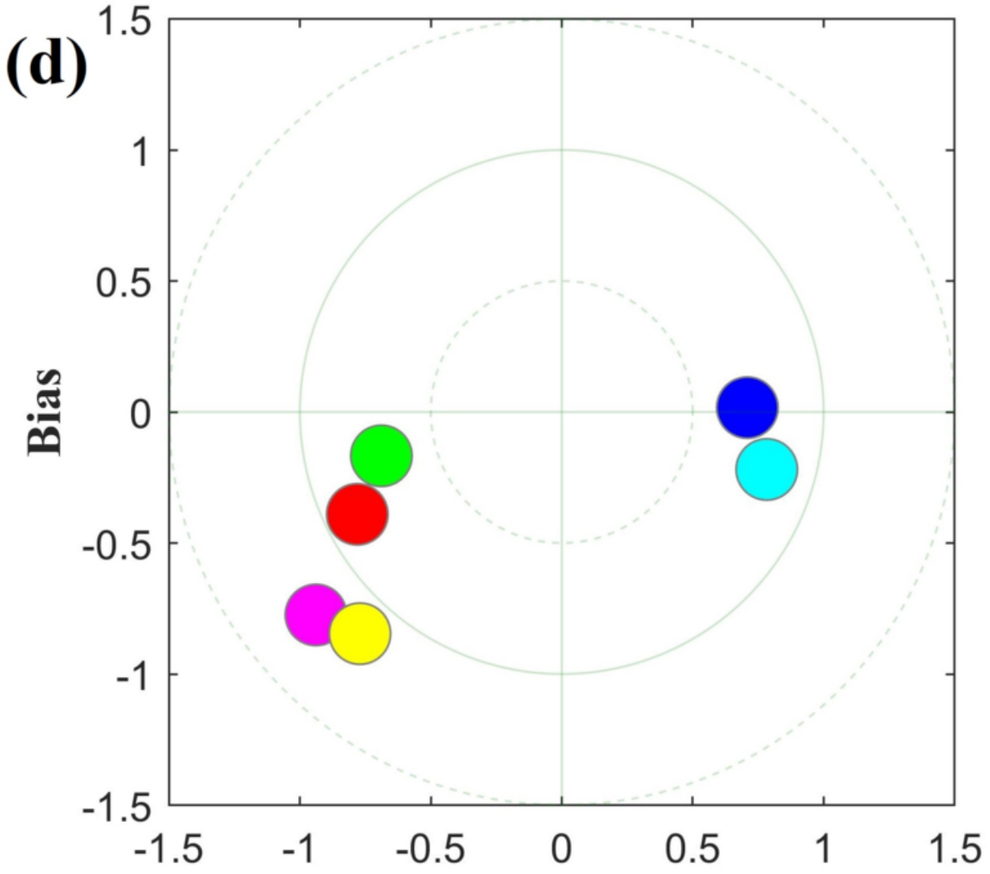
(d)
Bias
1.5
1
0.5
0
-0.5
-1
-1.5
Centered-RMSE

CB3.3C

CB4.3C

CB5.2

(a)

(b)

(c)

LE2.2

ET5.2

(d)

(e)

Concentration [$\times 10^6$ Cell L^{-1}]

0 1 2 3 4

Jan Mar May Jul Sep Nov Jan

Month

Obs

RCA

Jan
Feb
Mar
Apr
May
Jun
Jul
Aug
Sep
Oct
Nov
Dec
(a)
(b)
(c)
(d)
(e)
(f)
(g)
(h)
(i)
(j)
(k)
(l)
39.5
39
38.5
38
37.5
37
Latitude
-77 -76.5 -76
Longitude
1.5
1.2
0.9
0.6
0.3
0
Concentration [×10^6 Cell L^-1]

Jan
Feb
Mar
Apr
May
Jun
Jul
Aug
Sep
Oct
Nov
Dec
(a)
(b)
(c)
(d)
(e)
(f)
(g)
(h)
(i)
(j)
(k)
(l)
0.2 m s^{-1}
Depth [m]
10
20
30
300 250 200 150 100 50 0
Distance from Bay Mouth [km]
1 0.8 0.6 0.4 0.2 0
2 1.6 1.2 0.8 0.4 0
Concentration [$\times 10^6$ Cell L^{-1}]

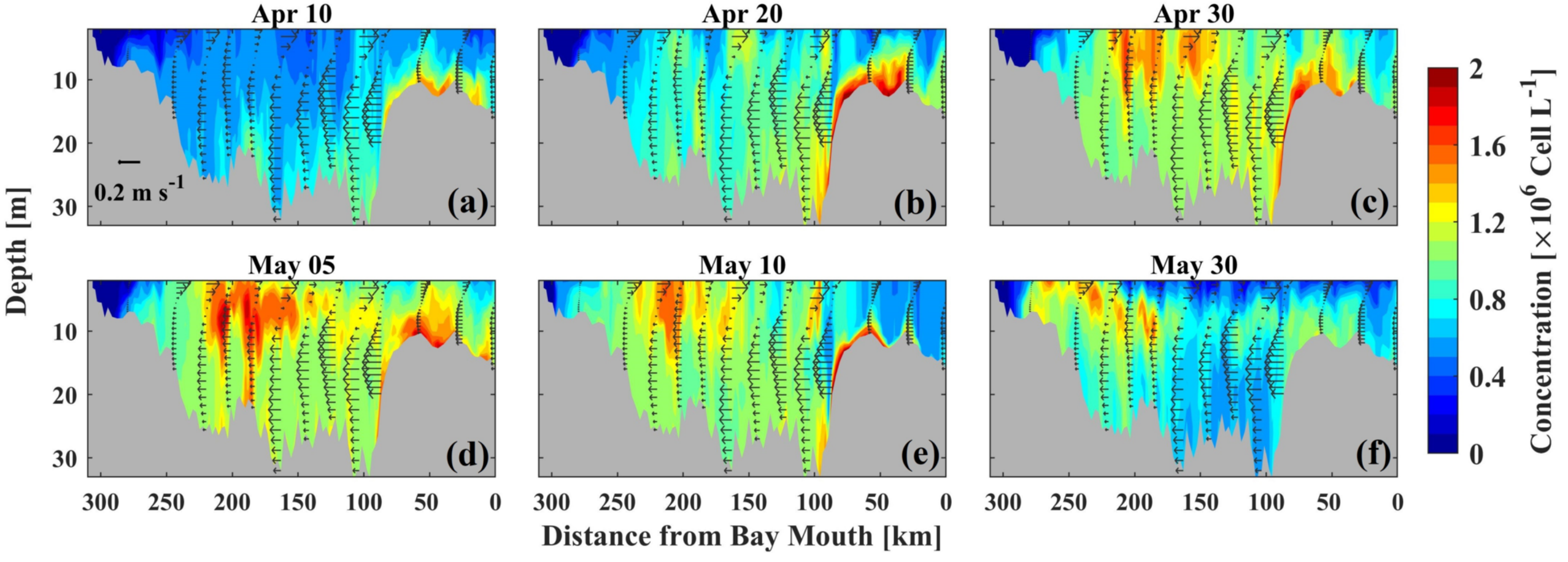
Apr 10
Apr 20
Apr 30
May 05
May 10
May 30
0.2 m s-1
(a)
(b)
(c)
(d)
(e)
(f)
Depth [m]
10
20
30
300
250
200
150
100
50
0
Distance from Bay Mouth [km]
2
1.6
1.2
0.8
0.4
0
Concentration [×10^6 Cell L^-1]

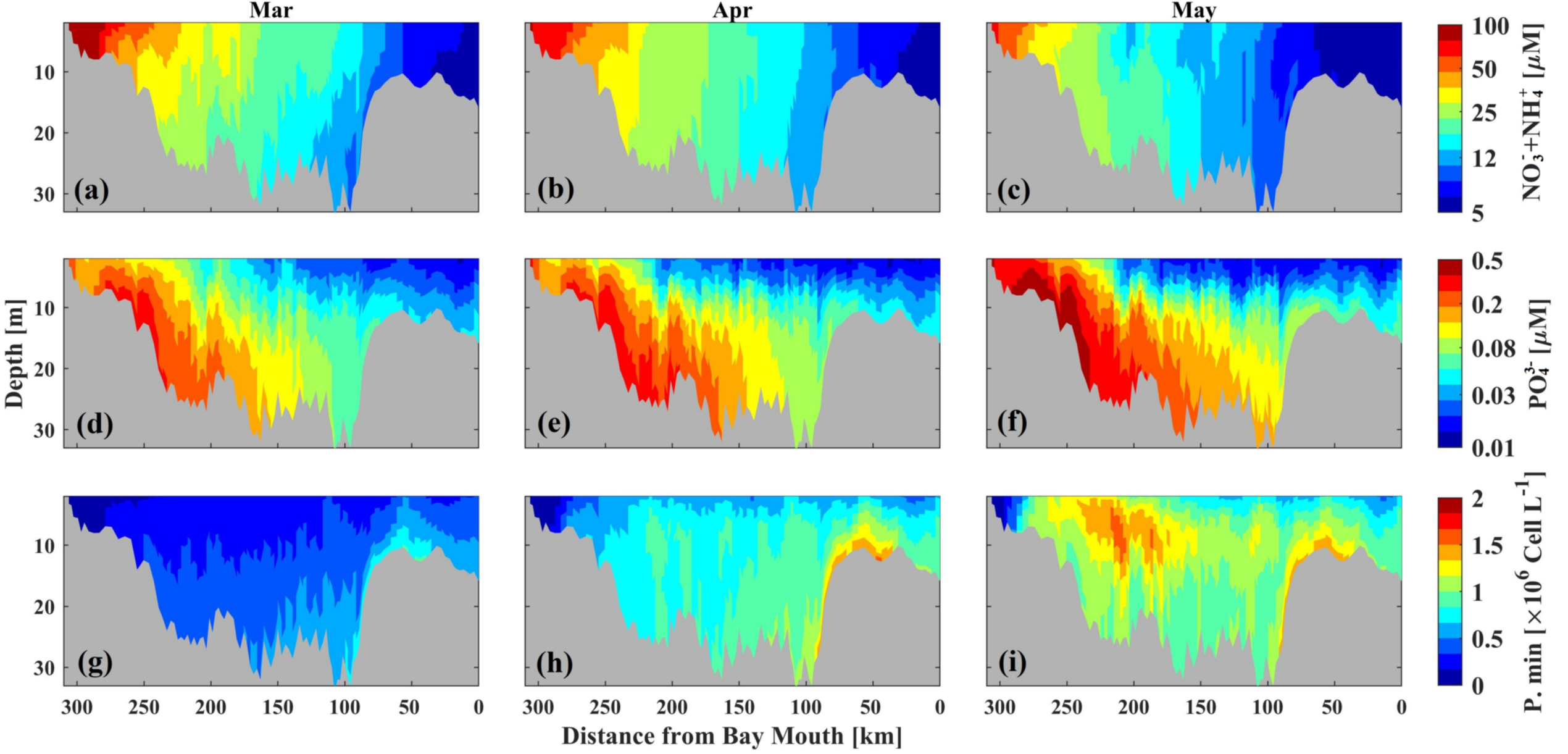
Mar
Apr
May
(a)
(b)
(c)
(d)
(e)
(f)
(g)
(h)
(i)
Depth [m]
10
20
30
300
250
200
150
100
50
0
Distance from Bay Mouth [km]
100
50
25
12
5
$NO_3^-+NH_4^+$ [μM]
0.5
0.2
0.08
0.03
0.01
PO_4^{3-} [μM]
2
1.5
1
0.5
0
P. min [$\times 10^6$ Cell L^{-1}]

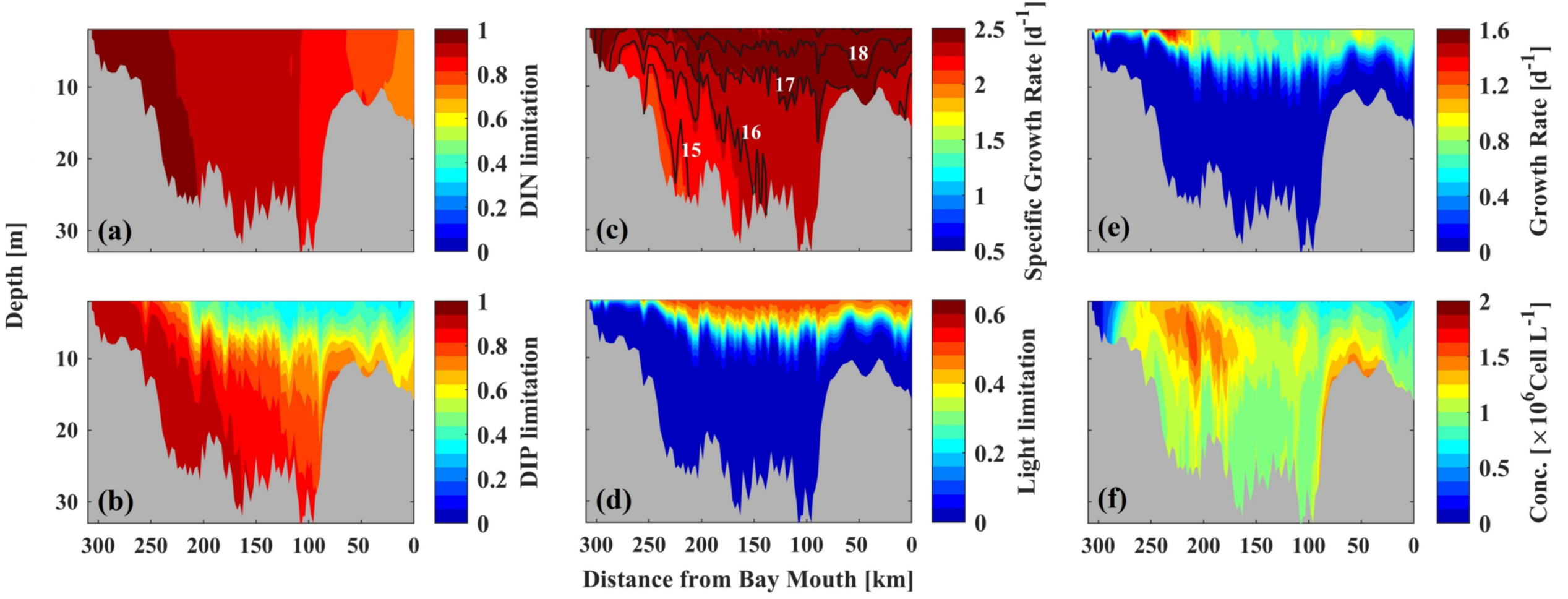
Depth [m]
10
20
30
(a)
(b)
(c)
(d)
(e)
(f)
15
16
17
18
1
0.8
0.6
0.4
0.2
0
DIN limitation
DIP limitation
2.5
2
1.5
1
0.5
Specific Growth Rate [d^{-1}]
0.6
0.4
0.2
0
Light limitation
1.6
1.2
0.8
0.4
0
Growth Rate [d^{-1}]
2
1.5
1
0.5
0
Conc. [×10^{6}Cell L^{-1}]
300 250 200 150 100 50 0
Distance from Bay Mouth [km]

(a) Temperature [^{o}C]

(b) Specific Growth Rate [d^{-1}]

(c) Nutrient Limitation

(d) Light Limitation

(e) Growth Rate [mgC L^{-1} d^{-1}]

(f) Grazing Rate [mgC L^{-1} d^{-1}]

(g) Respiration Rate [mgC L^{-1} d^{-1}]

(h) P. min. [$\times 10^{6}$Cell L^{-1}]

01 02 03 04 05 06 07 08 09 10 11 12 01

Month of 2006

Ctrl

Without DIN limitation

Without DIP limitation

(a)

(b)

(c)

Latitude

39.5
39
38.5
38
37.5
37

-77 -76.5 -76

Longitude

Concentration [$\times 10^6$ Cell L^{-1}]

5
4
3
2
1
0

(d)

(e)

(f)

Concentration [$\times 10^6$ Cell L^{-1}]

7
6
5
4
3
2
1
0

Jan Mar May Jul Sep Nov

Month of 2006

CB3.3C

(a)

Obs
Ctrl
Salin. exp
Optimal T=25°C

(b)

Obs
0.5×ini
Ctrl
1.5×ini
2.0×ini
3.0×ini

(c)

Obs
K_{mp}=0.001μM
Ctrl
K_{mp}=0.1μM
K_{mp}=1μM

Concentration [×10^6 Cell L^-1]

Jan
Mar
May
Jul
Sep
Nov
Jan

Month of 2006

2002 Average
2003 Wet
2004 Wet
2005 Wet
2006 Dry
2007 Dry
2008 Dry
2009 Dry
2010 Wet
2011 Wet
Latitude
Longitude
39.5
39
38.5
38
37.5
37
-77
-76.5
-76
Concentration [$\times 10^6$ Cell L^{-1}]
1.4
1.2
1
0.8
0.6
0.4

Table 1. Values of the parameters used in the *P. minimum* model.

Variable Name	Variable Value	Unit	References	Range of reported values
G_p	2.5	d^{-1}	Smayda (1996) and references reviewed in Heil et al. (2005)	0.12-3.54
α	0.019	ly^{-1}	Harding et al. (2002)	0.007-0.027
K_{mn}	1.0	μM N	Taylor et al. (2006) Glibert et al. (2012)	0.54-23.3
K_{mp}	0.03	μM P	Cembella et al. (1984) Ou et al. (2008) Jiang et al. (2019)	0.0003-1.96
T_{opt}	20	^{o}C	Tyler and Seliger (1981) Grzebyk and Berland (1996) Lomas and Glibert (1999) Tango et al. (2005)	19.0-25.0
β_1	0.007		Tyler and Seliger (1981) Grzebyk and Berland (1996) Lomas and Glibert (1999)	0.004-0.01
β_2	0.02			0.01-0.035
k_{gz}	0.1	d^{-1}	Johnson et al. (2003) Dam and Colin (2005)	$k_{gz}*\theta_{gz}^{(T-20)}$=[0.15-4.0]
θ_{gz}	1.15			
k_{rb}	0.1	d^{-1}	Heil (2005)	$k_{gz}*\theta_{gz}^{(T-20)}$=[0.05-0.1]
θ_{rb}	1.15			

Table 2. Correlation coefficient (r), root mean square error (RMSE), skill, mean absolute error, and mean error for model-data comparison of *P. minimum* cell density for 2006. Both model and observational data were monthly averaged for these comparisons.

	CB3.3C	*CB4.3C*	*CB5.2*	*LE2.2*	*ET5.2*
r	0.86	0.86	0.52	0.64	0.64
RMSE ($\times 10^6$ cell L^{-1})	0.26	0.20	0.33	0.86	1.18
Skill	0.90	0.92	0.23	0.69	0.57
Mean Absolute Error ($\times 10^6$ cell L^{-1})	0.21	0.16	0.22	0.52	0.74
Mean Error ($\times 10^6$ cell L^{-1})	-0.07	0.00	-0.18	0.20	0.57

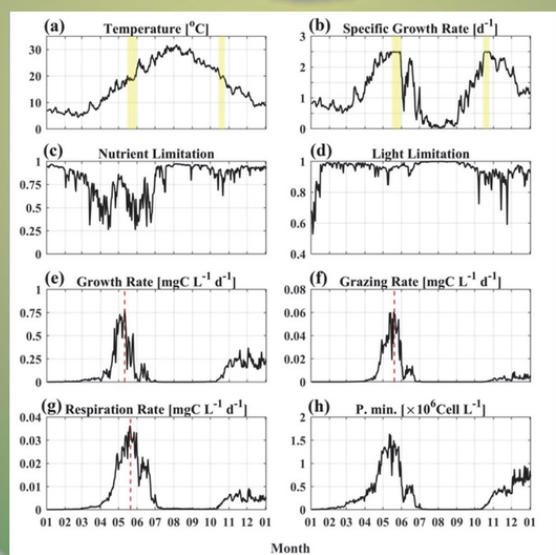
(a) Temperature [°C]
(b) Specific Growth Rate [d-1]
(c) Nutrient Limitation
(d) Light Limitation
(e) Growth Rate [mgC L-1 d-1]
(f) Grazing Rate [mgC L-1 d-1]
(g) Respiration Rate [mgC L-1 d-1]
(h) P. min. [×10^6Cell L-1]
01 02 03 04 05 06 07 08 09 10 11 12 01
Month